DISCRETE AND CONTINUOUS
DYNAMICAL SYSTEMS SERIES B

doi:10.3934/dcdsb.2020158

ENHANCED BACKSCATTERING OF A PARTIALLY COHERENT FIELD FROM AN ANISOTROPIC RANDOM LOSSY MEDIUM

Josselin Garnier

CMAP, CNRS, Ecole polytechnique, Institut Polytechnique de Paris
91128 Palaiseau Cedex, France

Knut Sølna*

Department of Mathematics
University of California, Irvine CA 92697, USA

(Communicated by Grégoire Allaire)

Abstract. The weak localization or enhanced backscattering phenomenon has received a lot of attention in the literature. The enhanced backscattering cone refers to the situation that the wave backscattered by a random medium exhibits an enhanced intensity in a narrow cone around the incoming wave direction. This phenomenon can be analyzed by a formal path integral approach. Here a mathematical derivation of this result is given based on a system of equations that describes the second-order moments of the reflected wave. This system derives from a multiscale stochastic analysis of the wave field in the situation with high-frequency waves and propagation through a lossy medium with fine scale random microstructure. The theory identifies a duality relation between the spreading of the wave and the enhanced backscattering cone. It shows how the cone, its regularity and width relate to the statistical structure of the random medium. We discuss how this information in particular can be used to estimate the internal structure of the random medium based on observations of the reflected wave.

1. **Introduction.** When a wave beam is impinging on a random halfspace or medium the reflected field can be decomposed into many plane waves with the decomposition over direction or wavevector being random. That is, the reflected wave is random and generated by the fluctuations in the random medium and it can be decomposed into plane wave components with random weights. Here we consider the question about what information about the random medium is imprinted in the distribution of the reflected wave or these random weights. In answering this question the first point to be made is a fascinating physical phenomenon referred to as weak localization or enhanced backscattering. In fact the intensity of the reflected wave in the reverse of the main incoming direction (the backscattered direction) is stronger than in the other directions. In weak localization, interference of the direct and reverse paths leads to a net reduction of light transport in the forward direction, similar to the weak localization phenomenon for electrons in disordered

2010 *Mathematics Subject Classification.* Primary: 35R60, 76B15; Secondary: 35Q99, 60F05.

Key words and phrases. Waves, random media, enhanced backscattering, asymptotic analysis, imaging, tissue, Paraxial equation.

This research is supported by AFOSR grant FA9550-18-1-0217, NSF grant 1616954.

* Corresponding author: Knut Sølna.

(semi)conductors and often seen as the precursor to Anderson (or strong) localization. Weak localization of light can be detected since it produces an enhancement of light intensity in the backscattered direction. This cone of directions of enhanced backscatter is called the cone of coherent backscattering. A physical interpretation for this phenomenon derives from constructive interferences between pairs of wave "paths" and reversed paths, see Figure 1. The sum of all these constructive interferences should give an enhancement factor of 2 in the backscattered direction. If the reflected wave is observed with an angle A compared to the backscattered direction, then the phase shift between the direct and reversed paths is $ke = kd \sin A$, where k is the wave number and d is the typical transverse size of a wave path. Therefore, constructive interference is possible if $kdA \leq 1$, determining the width of the cone. In fact in the simplest case this intuitive picture with an *enhanced backscattering (EBS) cone* holds true. This phenomenon was first observed and

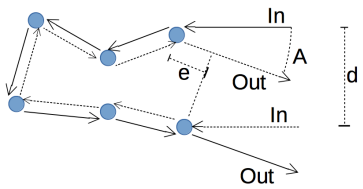

FIGURE 1. Physical interpretation of the scattering of a plane wave by a random medium. The output wave in direction A is the superposition of many different scattering paths. One of these paths is plotted as well as the reversed path. The phase difference between the two outgoing waves is $ke = kd \sin A$.

subject to intense study in the context of physics [2, 23, 38, 35, 32, 36, 37]. In [8, 9, 36] the enhanced backscattering is analyzed using diagrammatic expansions, while we here set forth a rigorous analysis in the paraxial regime. We will consider the case when there is backscattering from the medium itself which generates the enhanced backscattering cone, in the continuation of [11], while in [7, 13] we considered the situation with backscattering from respectively an incoherent interface and from microscopic particles like aerosol. We here consider a situation where we exploit the coherent part of the backscattered intensity, the enhanced backscattering cone, and seek configurations where the speckle noise can be mitigated. There are, however, other imaging modalities that seek to exploit the incoherent part in the speckle, the speckle correlations, for imaging [16, 17].

From the applications point of view, the enhanced backscattering cone has been put forward as a useful tool in medical imaging [40], in particular in spectroscopy for predicting the risk of colon carcinogenesis and colorectal cancer [21, 25] by using the shape of the cone to derive information about tissue statistics on the μm scale. Similar motivating applications can be found in the context of the turbulent atmosphere where one seeks to use backscattered wave energy to infer properties about the turbulence or presence of aerosols say [1, 5, 6].

In the case of biomedical applications medium anisotropy can be important. Biological cells may in particular be strongly anisotropic and associated with rough cell membranes generating backscattering. In [30] a common cell anisotropy factor of about 5 was reported, while in [19] the authors discuss backscattering from rough anisotropic cells. The enhanced backscattering cone has indeed been used

to detect such roughness and anomalous tissue associated with cancer, examples range from colon cancer [21], to lung cancer [27] and non-melanoma skin cancer [24]. Cone parameters like width, enhancement factor and wavelength dependence are used as markers to probe for cell carcinogenesis causing micro/nano-scale alterations. In the context of the turbulent atmosphere anisotropy can also be important and corresponds to rapid vertical index of refraction fluctuations driven by vertical temperature gradients.

Observations of the EBS cone is a challenging task, but important progress has been made by using sources with *low spatial coherence* which serves to broaden the cone and enhance the signal-to-noise ratio giving Low-coherence Enhanced Backscattering (LEBS) [25, 34]. Low spatial coherence in the incoming wave corresponds to probing with a transverse wave profile that exhibits fluctuations, as opposed to a plane wave profile. The independent transverse coherence structures serve to enhance the signal-to-noise ratio since they provide independent contributions to the cone profile and favors scattering events that serves to broaden the cone, moreover, partially eliminate the speckle noise. The signal-to-noise ratio can be further enhanced by temporal coherence [20]. Low Coherence Enhanced Backscattering also allows for depth selectivity since the depth range involved in the backscattering enhancement for a given angle can be controlled by the lateral coherence radius of the source [20, 22].

As a model for the statistics of the microstructural fluctuations in the index of refraction in biological tissue or for atmospheric turbulence the Matérn covariance function has played an important role [18]. This covariance function describes in particular turbulent media with power law decay of the correlations. Media of this type are also referred to as fractal [31, 39]. The power law parameter governs the roughness of the medium and this medium feature has been identified as important to characterize biological tissue anomaly [33]. We analyze from first principles how the statistics of the microstructure affects the cone shape, producing an explicit connection in between biological tissue structure or atmospheric conditions and the enhanced backscattering cone. In our analysis, motivated by the applications discussed, we will model the microstructure as anisotropic and use the Matérn covariance function to describe its statistics. The enhanced backscattering cone will depend on the incoming beam radius and its coherence properties [3, 21] and we analyze explicitly here this connection.

The outline of the paper is as follows. In Section 2 we articulate the scaling assumptions which correspond to beam propagation in an attenuating anisotropic random medium. In Sections 3-4 we characterize the backscattered power and intensity as a function of position. We address the enhanced backscattering phenomenon in the small Fresnel number regime in Section 5. In Section 6 we analyze the form of the backscattered intensity as a function of angle and in particular the enhancement cone in the case of the Matérn covariance function for the medium statistics. We finish with some concluding remarks in Section 8.

2. **Waves in a random medium.**

We consider the scalar time-harmonic $d+1$-dimensional wave equation

$$\frac{\omega^2}{\varepsilon^4 c^\varepsilon(\boldsymbol{x},z)^2}u^\varepsilon + \Delta u^\varepsilon + \frac{i\omega\sigma^\varepsilon(\boldsymbol{x},z)}{\varepsilon^2 c^\varepsilon(\boldsymbol{x},z)^2}u^\varepsilon = -f^\varepsilon(\boldsymbol{x},z)\,, \tag{1}$$

where u^ε is the scalar wave field, c^ε is the propagation speed of the medium, σ^ε is the attenation of the medium, ω/ε^2 is the operating frequency, and $(\boldsymbol{x},z)\in\mathbb{R}^d\times\mathbb{R}$ are

the space coordinates. Here ε is a small parameter that characterizes the paraxial regime, in which the wavelength is much smaller than the radius of the source, which is itself much smaller than the typical propagation distance. The source is modeled by the forcing term f^ε:

$$f^\varepsilon(\boldsymbol{x},z) = \nabla\cdot \boldsymbol{F}^\varepsilon(\boldsymbol{x},z), \qquad \boldsymbol{F}^\varepsilon(\boldsymbol{x},z) = F\Big(\frac{\boldsymbol{x}}{\varepsilon}\Big)\delta(z)\boldsymbol{e}_z\,, \tag{2}$$

with $\boldsymbol{e}_z$ the unit vector pointing in the z-direction. Here we shall focus on reflection from a random region occupying the interval $z\in(-L,0)$ (or the half-space $z\in(-\infty,0)$) with the source f^ε located at $z=0^+$. The parameterization is motivated by waves probing an inhomogeneous medium and z is the main probing direction. In the biological applications referred to above this is the direction corresponding to propagation into the tissue while it is the vertical direction in the context of propagation through atmospheric turbulence. Here we shall refer to waves propagating in a direction with a positive z component as right-propagating waves.

2.1. **Random and attenuating medium.** We consider a scaling where the random medium fluctuations vary relatively rapidly in space while the "background" medium is constant. We consider the following anisotropic model for the fluctuations of the propagation speed and the attenuation:

$$\frac{1}{c^\varepsilon(\boldsymbol{x},z)^2} = \frac{1}{c_o^2}\begin{cases} 1+\varepsilon\nu(\boldsymbol{x}/\varepsilon, z/\varepsilon^2) \text{ if } z\in(-L,0)\,,\\ 1 \text{ otherwise }\,, \end{cases} \tag{3}$$

$$\frac{\sigma^\varepsilon(\boldsymbol{x},z)}{c^\varepsilon(\boldsymbol{x},z)^2} = \frac{\sigma_o}{c_o^2}\begin{cases} 1+\varepsilon\mu(\boldsymbol{x}/\varepsilon, z/\varepsilon^2) \text{ if } z\in(-L,0)\,,\\ 0 \text{ otherwise }\,, \end{cases} \tag{4}$$

where c_o and σ_o are positive constants. As mentioned in the introduction, the anisotropy in the medium with relatively rapid fluctuations in the z-direction can come from anisotropic cell structure in the case of biological tissue or from rapid vertical index of refraction fluctuations driven by vertical temperature gradients in the context of the turbulent atmosphere. The random fields $\nu(\boldsymbol{x},z)$ and $\mu(\boldsymbol{x},z)$ model the spatial fluctuations of the medium and we assume that they are zero-mean, stationary, $(d+1)$-dimensional random processes and that they satisfy strong mixing conditions in the z-direction. We define the autocorrelation function of the fluctuations of the medium and its Fourier transform by

$$C(\boldsymbol{x},z) = \mathbb{E}[\nu(\boldsymbol{x}'+\boldsymbol{x},z'+z)\nu(\boldsymbol{x}',z')]\,, \tag{5}$$

$$\widehat{C}(\boldsymbol{k},k) = \int_{\mathbb{R}^d}\int_{-\infty}^{\infty} C(\boldsymbol{x},z)e^{-i(\boldsymbol{k}\cdot\boldsymbol{x}+kz)}dzd\boldsymbol{x}\,. \tag{6}$$

We remark that the medium is specified as being matched at the boundaries of the random region $z\in(-L,0)$ so that the wave speed in the complement of the random region $z<-L$ and $z>0$ coincides with the background wave speed in the random region $z\in(-L,0)$ [10].

2.2. **Wave mode decomposition.** Our objective is to characterize the reflected wave field. Our first task is to identify equations that give a convenient description of coupling between different wave modes. The complex amplitudes $\check{a}^\varepsilon$ and $\check{b}^\varepsilon$ of

the right-propagating and left-propagating modes are defined by

$$\check{a}^\varepsilon(\boldsymbol{x},z) = \Big(\frac{1}{2}u^\varepsilon(\varepsilon\boldsymbol{x},z) + \frac{c_o\varepsilon^2}{2i\omega}\frac{\partial u^\varepsilon}{\partial z}(\varepsilon\boldsymbol{x},z)\Big)e^{-i\frac{\omega}{c_o}\frac{z}{\varepsilon^2}}\,, \tag{7}$$

$$\check{b}^\varepsilon(\boldsymbol{x},z) = \Big(\frac{1}{2}u^\varepsilon(\varepsilon\boldsymbol{x},z) - \frac{c_o\varepsilon^2}{2i\omega}\frac{\partial u^\varepsilon}{\partial z}(\varepsilon\boldsymbol{x},z)\Big)e^{i\frac{\omega}{c_o}\frac{z}{\varepsilon^2}}\,. \tag{8}$$

They are such that the wave field has the form:

$$u^\varepsilon(\boldsymbol{x},z) = \check{a}^\varepsilon\big(\frac{\boldsymbol{x}}{\varepsilon},z\big)e^{i\frac{\omega}{c_o}\frac{z}{\varepsilon^2}} + \check{b}^\varepsilon\big(\frac{\boldsymbol{x}}{\varepsilon},z\big)e^{-i\frac{\omega}{c_o}\frac{z}{\varepsilon^2}}\,, \tag{9}$$

and they also satisfy the condition that serves to correctly decompose the wave

$$\frac{\partial\check{a}^\varepsilon}{\partial z}e^{i\frac{\omega}{c_o}\frac{z}{\varepsilon^2}} + \frac{\partial\check{b}^\varepsilon}{\partial z}e^{-i\frac{\omega}{c_o}\frac{z}{\varepsilon^2}} = 0\,. \tag{10}$$

In the homogeneous case $\nu = \mu = 0$ the ansatz (7-8) gives a decomposition into uncoupled right- and left-propagating modes, the mode amplitudes $\check{a}^\varepsilon$ and $\check{b}^\varepsilon$ are constant in the half-space $z < 0$ and they are determined by the source. In the layered case $\nu = \nu(z)$ and $\mu = \mu(z)$ the ansatz gives a decomposition into right- and left-propagating modes that couple via a zero-mean random coupling matrix. The problem moreover decomposes into distinct mode problems parameterized by the transverse wavevector $\boldsymbol{k}$ [10]. In the general case with $\nu = \nu(\boldsymbol{x},z)$ and $\mu = \mu(\boldsymbol{x},z)$ the modes are coupled via a zero-mean coupling "matrix" which involves modes of all transverse wavevectors so that the coupling matrix is in fact a coupling operator [12, 14] as shown below.

By substituting the ansatz (7-8) into Eq. (1) and by using the medium model in (3-4) we obtain the following coupled mode equations for $z \in (-L,0)$:

$$\frac{d\check{a}^\varepsilon}{dz} = \mathcal{L}^\varepsilon(\boldsymbol{x},z)\check{a}^\varepsilon + e^{-2i\frac{i\omega}{c_o}\frac{z}{\varepsilon^2}}\mathcal{L}^\varepsilon(\boldsymbol{x},z)\check{b}^\varepsilon\,, \tag{11}$$

$$\frac{d\check{b}^\varepsilon}{dz} = -e^{2i\frac{i\omega}{c_o}\frac{z}{\varepsilon^2}}\mathcal{L}^\varepsilon(\boldsymbol{x},z)\check{a}^\varepsilon - \mathcal{L}^\varepsilon(\boldsymbol{x},z)\check{b}^\varepsilon\,, \tag{12}$$

where

$$\mathcal{L}^\varepsilon(\boldsymbol{x},z) = \frac{i\omega}{2c_o\varepsilon}\nu\big(\frac{z}{\varepsilon^2},\boldsymbol{x}\big) + \frac{ic_o}{2\omega}\Delta_\perp - \frac{\sigma_o}{2c_o}\Big(1+\varepsilon\mu\big(\frac{z}{\varepsilon^2},\boldsymbol{x}\big)\Big)\,, \tag{13}$$

and $\Delta_\perp$ is the transverse Laplacian. We describe below how this formulation leads to a description of the statistics of the reflected wave via the introduction of a reflection operator. To describe the problem satisfied by the reflection operator we next discuss appropriate boundary conditions.

2.3. **Boundary conditions.** The mode amplitudes $\check{a}^\varepsilon$ and $\check{b}^\varepsilon$ satisfy the system (11-12) in the random region $z \in (-L,0)$. This system can be supplemented by boundary conditions corresponding to the presence of the source term (2) in the plane $z = 0$. In the regions $z \in (-\infty,-L)$ and $z \in (0,\infty)$ the medium is homogeneous. Then, taking into account the fact that there is no source in $(-\infty,-L)$, we find that the right-going mode amplitudes $\check{a}^\varepsilon$ are zero in this half-space:

$$\check{a}^\varepsilon(\boldsymbol{x},-L) = 0\,. \tag{14}$$

Moreover, taking into account the fact that there is no source in $(0,\infty)$, we find that the left-going mode amplitudes $\check{b}^\varepsilon$ are zero in this half-space. The jump conditions accross the source interface $z = 0$ then give the relations

$$\check{a}^\varepsilon(\boldsymbol{x},0^+) - \check{a}^\varepsilon(\boldsymbol{x},0^-) = -\frac{1}{2}F(\boldsymbol{x})\,, \quad \check{b}^\varepsilon(\boldsymbol{x},0^-) = \check{b}_0(\boldsymbol{x}) := \frac{1}{2}F(\boldsymbol{x})\,. \tag{15}$$

We will consider two types of sources, coherent and partially coherent:
- A coherent source which has a smooth deterministic transverse profile (say, Gaussian) and a main angle of incidence (determined by the transverse wavector $\boldsymbol{k}_0$):

$$F(\boldsymbol{x}) = \exp\Big(-\frac{|\boldsymbol{x}|^2}{2r_0^2} + i\boldsymbol{k}_0\cdot\boldsymbol{x}\Big)\,, \tag{16}$$

where r_0 is the initial radius and $\boldsymbol{k}_0$ is the incident transverse wavevector which together with the rapid phase modulation in (9) determines the full wavevector $(\boldsymbol{k}_0, \omega/c_o)$ giving the direction of propagation, in particular the angle $\mathrm{atan}(|\boldsymbol{k}_0/(\omega/c_o)|)$ with respect to the z-axis.
- A partially coherent source which has random fluctuations within an envelope. A convenient model is the Gauss-Schell model:

$$\Big\langle F\big(\boldsymbol{x}+\frac{\boldsymbol{y}}{2}\big)\overline{F}\big(\boldsymbol{x}-\frac{\boldsymbol{y}}{2}\big)\Big\rangle = \exp\Big(-\frac{|\boldsymbol{x}|^2}{r_0^2} - \frac{|\boldsymbol{y}|^2}{4\rho_0^2} + i\boldsymbol{k}_0\cdot\boldsymbol{y}\Big)\,, \tag{17}$$

where ρ_0 ($\leq r_0$) is the initial correlation radius. Here and below $\langle\cdot\rangle$ means expectation with respect to the source distribution, which is assumed to be independent of the medium fluctuations, while we use the symbol $\mathbb{E}\,[\cdot]$ for the expectation with respect to the medium distribution. In the case that $\rho_0 = r_0$ this model in fact gives the fully coherent source in Eq. (16).

2.4. **Reflection operator.** We make use of an invariant imbedding step and introduce reflection and transmission operators. First, we define the transverse Fourier modes

$$\hat{a}^\varepsilon(\boldsymbol{k},z) = \int \check{a}^\varepsilon(\boldsymbol{x},z)e^{-i\boldsymbol{k}\cdot\boldsymbol{x}}\,d\boldsymbol{x}\,, \qquad \hat{b}^\varepsilon(\boldsymbol{k},z) = \int \check{b}^\varepsilon(\boldsymbol{x},z)e^{-i\boldsymbol{k}\cdot\boldsymbol{x}}\,d\boldsymbol{x}\,, \tag{18}$$

and make the ansatz

$$\hat{b}^\varepsilon(\boldsymbol{k},-L) = \int \hat{\mathcal{T}}^\varepsilon(\boldsymbol{k},\boldsymbol{k}',z)\hat{b}^\varepsilon(\boldsymbol{k}',z)\,d\boldsymbol{k}'\,, \tag{19}$$

$$\hat{a}^\varepsilon(\boldsymbol{k},z) = \int \hat{\mathcal{R}}^\varepsilon(\boldsymbol{k},\boldsymbol{k}',z)\hat{b}^\varepsilon(\boldsymbol{k}',z)d\boldsymbol{k}'\,. \tag{20}$$

We refer to [12] for a detailed dicussion of this ansatz and mention that the random medium produces transmission and reflector operators that are random in the sense that they depend on the realization of the random medium. In the parameterization we use here they depend on the medium in between the depth z of evaluation and the depth $-L$ of the termination of the random slab and models respectively transmission through and reflection from this part of the slab. For $\hat{b}^\varepsilon(\boldsymbol{k}',0^-)$ giving the incoming wave (see Eq. (15)), $\hat{\mathcal{T}}^\varepsilon(\boldsymbol{k},\boldsymbol{k}',0)$ maps it to the wave $\hat{b}^\varepsilon(\boldsymbol{k},-L)$ transmitted to $z=-L$, while $\hat{\mathcal{R}}^\varepsilon(\boldsymbol{k},\boldsymbol{k}',0)$ maps it to the wave $\hat{a}^\varepsilon(\boldsymbol{k},0^-)$ reflected from the random medium.

The backscattering from for instance biological tissue or the turbulent atmosphere is weak and we shall make an assumption about weak backscattering corresponding to the scale of variation of the medium in the z-direction being large relative to the wavelength, and the medium fluctuations being smooth so that the autocorrelation function $\widehat{C}$ decays rapidly. This can be expressed by the hypothesis

$$\frac{\widehat{C}(\boldsymbol{k},2\omega/c_o)}{\widehat{C}(\boldsymbol{0},0)} \leq \delta \ll 1\,, \quad \forall \boldsymbol{k}\in\mathbb{R}^d\,. \tag{21}$$

The reflection operator has been studied in detail in [11] when there is no attenuation and weak backscattering. The proof can be revisited in the presence of attenuation and we get the following proposition (see Appendix A).

Proposition 1. *We introduce the dimensionless autocorrelation function $\mathcal{C}$ of the random medium:*

$$C(\boldsymbol{x},z)=\sigma^2\mathcal{C}\Big(\frac{\boldsymbol{x}}{\ell_x},\frac{z}{\ell_z}\Big)\,, \tag{22}$$

where ℓ_z (respectively ℓ_x) is the longitudinal (respectively transverse) correlation radius of the random fluctuations, and σ is the standard deviation of the fluctuations. We denote by $\widehat{\mathcal{C}}_K(\boldsymbol{\mu})$ and by $\check{\mathcal{C}}_K(\boldsymbol{\lambda})$ the full and partial Fourier transforms

$$\widehat{\mathcal{C}}_K(\boldsymbol{\mu})=\int_{-\infty}^{\infty}\int_{\mathbb{R}^d}\mathcal{C}(\boldsymbol{\lambda},\zeta)e^{-iK\zeta-i\boldsymbol{\mu}\cdot\boldsymbol{\lambda}}d\boldsymbol{\lambda}d\zeta\,,\qquad \check{\mathcal{C}}_K(\boldsymbol{\lambda})=\int_{-\infty}^{\infty}\mathcal{C}(\boldsymbol{\lambda},\zeta)e^{-iK\zeta}d\zeta\,. \tag{23}$$

We have as $\varepsilon\to 0$ and in the weak backscattering regime (21)

$$\mathbb{E}\Big[\hat{\mathcal{R}}^\varepsilon(\boldsymbol{k}_0'+\boldsymbol{k},\boldsymbol{k}_0',z)\overline{\hat{\mathcal{R}}^\varepsilon}(\boldsymbol{k}_1'+\boldsymbol{k}',\boldsymbol{k}_1',z)\Big]\stackrel{\varepsilon\to 0}{\longrightarrow}\delta(\boldsymbol{k}'-\boldsymbol{k})D_{\boldsymbol{k}_0',\boldsymbol{k}_1',\boldsymbol{k}}(z)\,, \tag{24}$$

where the cross spectral density $D_{\boldsymbol{k}_0',\boldsymbol{k}_1',\boldsymbol{k}}(z)$ is of the form

$$\begin{aligned}D_{\boldsymbol{k}_0',\boldsymbol{k}_1',\boldsymbol{k}}(z)\;&=\;\overline{D}_o\exp\Big[-i(\boldsymbol{k}_0'-\boldsymbol{k}_1')\cdot(\boldsymbol{k}_0'+\boldsymbol{k}_1'+\boldsymbol{k})\frac{c_oz}{\omega}\Big]\\&\quad\times\mathcal{D}\Big((\boldsymbol{k}_0'-\boldsymbol{k}_1')\ell_x,(\boldsymbol{k}_0'+\boldsymbol{k}_1'+\boldsymbol{k})\ell_x,\boldsymbol{k}\ell_x,\frac{z}{L_{\rm att}}\Big)\,,\end{aligned} \tag{25}$$

with

$$\overline{D}_o=\frac{\sigma^2\ell_z\ell_x^dL_{\rm att}\check{\mathcal{C}}_{K_z}(\boldsymbol{0})}{4(2\pi)^{d-2}\lambda_o^2}\,,\qquad \lambda_o=\frac{2\pi c_o}{\omega}\,,\qquad L_{\rm att}=\frac{c_o}{2\sigma_o}\,. \tag{26}$$

The dimensionless cross spectral density $\mathcal{D}(\boldsymbol{u},\boldsymbol{v},\boldsymbol{w},\zeta)$ for $\zeta\in(-\zeta_L,0)$ solves

$$\begin{aligned}&\frac{d\mathcal{D}(\boldsymbol{u},\boldsymbol{v},\boldsymbol{w},\zeta)}{d\zeta}=\frac{\widehat{\mathcal{C}}_{K_z}(\boldsymbol{w})}{\check{\mathcal{C}}_{K_z}(\boldsymbol{0})}e^{i\alpha\boldsymbol{u}\cdot\boldsymbol{v}\zeta}-\mathcal{D}(\boldsymbol{u},\boldsymbol{v},\boldsymbol{w},\zeta)-\frac{2\beta}{(2\pi)^d}\int\widehat{\mathcal{C}}_0(\boldsymbol{\mu})d\boldsymbol{\mu}\mathcal{D}(\boldsymbol{u},\boldsymbol{v},\boldsymbol{w},\zeta)\\&+\frac{\beta}{(2\pi)^d}\int\widehat{\mathcal{C}}_0(\boldsymbol{\mu})\left[e^{i\alpha\boldsymbol{\mu}\cdot\boldsymbol{v}\zeta}\mathcal{D}(\boldsymbol{u}-\boldsymbol{\mu},\boldsymbol{v},\boldsymbol{w}+\boldsymbol{\mu},\zeta)+e^{-i\alpha\boldsymbol{\mu}\cdot\boldsymbol{v}\zeta}\mathcal{D}(\boldsymbol{u}+\boldsymbol{\mu},\boldsymbol{v},\boldsymbol{w}+\boldsymbol{\mu},\zeta)\right]d\boldsymbol{\mu}\\&+\frac{\beta}{(2\pi)^d}\int\widehat{\mathcal{C}}_0(\boldsymbol{\mu})\left[e^{i\alpha\boldsymbol{\mu}\cdot\boldsymbol{u}\zeta}\mathcal{D}(\boldsymbol{u},\boldsymbol{v}-\boldsymbol{\mu},\boldsymbol{w}+\boldsymbol{\mu},\zeta)+e^{-i\alpha\boldsymbol{\mu}\cdot\boldsymbol{u}\zeta}\mathcal{D}(\boldsymbol{u},\boldsymbol{v}+\boldsymbol{\mu},\boldsymbol{w}+\boldsymbol{\mu},\zeta)\right]d\boldsymbol{\mu}\\&-\frac{\beta}{(2\pi)^d}\int\widehat{\mathcal{C}}_0(\boldsymbol{\mu})e^{-i\alpha\boldsymbol{\mu}\cdot\boldsymbol{u}\zeta}\Big[e^{-i\alpha\boldsymbol{\mu}\cdot(\boldsymbol{v}+\boldsymbol{\mu})\zeta}\mathcal{D}(\boldsymbol{u}+\boldsymbol{\mu},\boldsymbol{v}+\boldsymbol{\mu},\boldsymbol{w},\zeta)\\&\qquad+e^{i\alpha\boldsymbol{\mu}\cdot(\boldsymbol{v}+\boldsymbol{\mu})\zeta}\mathcal{D}(\boldsymbol{u}-\boldsymbol{\mu},\boldsymbol{v}+\boldsymbol{\mu},\boldsymbol{w},\zeta)\Big]d\boldsymbol{\mu}\,,\end{aligned} \tag{27}$$

starting from $\mathcal{D}(\boldsymbol{u},\boldsymbol{v},\boldsymbol{w},\zeta=-\zeta_L)=0$, where

$$\zeta_L=\frac{L}{L_{\rm att}},\qquad K_z=\frac{2\omega\ell_z}{c_o}\,. \tag{28}$$

The dimensionless parameters α and β are given by

$$\alpha=\frac{c_o^2}{2\sigma_o\omega\ell_x^2}=\frac{\lambda_oL_{\rm att}}{2\pi\ell_x^2},\qquad \beta=\frac{\omega^2\sigma^2\ell_z}{8c_o\sigma_o}=\frac{\pi^2\sigma^2\ell_zL_{\rm att}}{\lambda_o^2}\,. \tag{29}$$

The parameter α is the inverse of the Fresnel number at the transverse scale ℓ_x and for a propagation distance of the order of $L_{\rm att}$, and it characterizes the strength of diffraction. The parameter β is the ratio of the attenuation distance over the scattering mean free path, and it characterizes the strength of random forward

scattering for a propagation distance of the order of $L_{\rm att}$. In typical applications, both α and β are larger than one. This means that the wave can penetrate up to depths that are in the far-field or Fraunhofer diffraction regime ($\alpha \gg 1$), and that are deeper than the scattering mean free path ($\beta \gg 1$).

3. **Mean reflected power.** As a first application of Proposition 1, we compute the mean reflected power defined by:

$$P_{\rm tot}^\varepsilon = \int \big\langle \mathbb{E}[|\check{a}^\varepsilon(\boldsymbol{x},0)|^2]\big\rangle \, d\boldsymbol{x}\,. \tag{30}$$

Proposition 2. *The mean reflected power $P_{\rm tot}^\varepsilon$ as $\varepsilon \to 0$ and in the weak backscattering regime (21) has the limit $P_{\rm tot}$ which is given by*

$$P_{\rm tot} = \beta \check{\mathcal{C}}_{K_z}(\boldsymbol{0})\Big[\int \big\langle |\check{b}_0(\boldsymbol{x})|^2\big\rangle \, d\boldsymbol{x}\Big]\Big[1-\exp(-L/L_{\rm att})\Big]\,, \tag{31}$$

where $\check{b}_0(\boldsymbol{x}) = \frac{1}{2}F(\boldsymbol{x})$ stands for the incoming wave (15).

Proof. Using Parseval's formula we have

$$\begin{aligned} P_{\rm tot}^\varepsilon &= \frac{1}{(2\pi)^d}\int \big\langle \mathbb{E}[|\hat{a}^\varepsilon(\boldsymbol{k},0)|^2]\big\rangle \, d\boldsymbol{k} \\ &= \frac{1}{(2\pi)^d}\iiint \mathbb{E}\big[\hat{\mathcal{R}}^\varepsilon(\boldsymbol{k},\boldsymbol{k}',0)\overline{\hat{\mathcal{R}}^\varepsilon}(\boldsymbol{k},\boldsymbol{k}'',0)\big]\Big\langle \hat{b}_0(\boldsymbol{k}')\overline{\hat{b}_0}(\boldsymbol{k}'')\Big\rangle \, d\boldsymbol{k}d\boldsymbol{k}'d\boldsymbol{k}''\,, \end{aligned}$$

where $\hat{b}_0(\boldsymbol{k})$ stands for the incoming wave. By the convergence (24) the mean reflected power $P^\varepsilon(\omega)$ has the limit $P(\omega)$ as $\varepsilon \to 0$ given by

$$P_{\rm tot} = \frac{1}{(2\pi)^d}\iint D_{\boldsymbol{k}',\boldsymbol{k}',\boldsymbol{k}-\boldsymbol{k}'}(0)\Big\langle |\hat{b}_0(\boldsymbol{k}')|^2\Big\rangle \, d\boldsymbol{k}d\boldsymbol{k}'\,.$$

Using the identity (25) this can also be written as

$$P_{\rm tot} = \frac{\overline{D}_o \ell_x^{-d}}{(2\pi)^d}\int \mathcal{E}(2\boldsymbol{k}'\ell_x,0)\Big\langle |\hat{b}_0(\boldsymbol{k}')|^2\Big\rangle \, d\boldsymbol{k}'\,,$$

where $\mathcal{E}(\boldsymbol{v},\zeta) = \int \mathcal{D}(\boldsymbol{0},2\boldsymbol{v}+\boldsymbol{w},\boldsymbol{w},\zeta)d\boldsymbol{w}$. Then, using the system of coupled differential equations (27), we get that the function $\mathcal{E}(\boldsymbol{v},\zeta)$ satisfies

$$\frac{d\mathcal{E}(\boldsymbol{v},\zeta)}{d\zeta} = (2\pi)^d - \mathcal{E}(\boldsymbol{v},\zeta) + \frac{\beta}{(2\pi)^d}\int \widehat{\mathcal{C}}_0(\boldsymbol{\mu})\Big[\mathcal{E}(\boldsymbol{v}+\boldsymbol{\mu},\zeta)-\mathcal{E}(\boldsymbol{v},\zeta)\Big]d\boldsymbol{\mu}\,,$$

because all but two of the terms of the right-hand side of (27) cancel when taking $(\boldsymbol{u},\boldsymbol{v},\boldsymbol{w}) \to (\boldsymbol{0},2\boldsymbol{v}+\boldsymbol{w},\boldsymbol{w})$ and integrating in $\boldsymbol{w}$. The initial condition is $\mathcal{E}(\boldsymbol{v},\zeta = -\zeta_L) = 0$ and the solution is the function $\mathcal{E}(\boldsymbol{v},\zeta) = (2\pi)^d(1-\exp(-\zeta_L-\zeta))$ independent of $\boldsymbol{v}$. We finally obtain that the mean reflected power is

$$P_{\rm tot} = \overline{D}_o \ell_x^{-d}\int \Big\langle |\hat{b}_0(\boldsymbol{k})|^2\Big\rangle \, d\boldsymbol{k}\big(1-\exp(-\zeta_L)\big)\,, \tag{32}$$

which also reads as (31). □

This proposition shows that, in the case of a random half-space or when $L \gg L_{\rm att}$, the mean reflected power is:

$$P_{\rm tot} = \beta \check{\mathcal{C}}_{K_z}(\boldsymbol{0})\Big[\int \big\langle |\check{b}_0(\boldsymbol{x})|^2\big\rangle \, d\boldsymbol{x}\Big]\,. \tag{33}$$

Note that we have

$$\beta\check{\mathcal{C}}_{K_z}(\boldsymbol{0}) = \frac{\pi^2 L_{\rm att}}{2\lambda_o}\int_{-\infty}^{\infty} \mathbb{E}\left[\nu(\boldsymbol{0},0)\nu(\boldsymbol{0},\zeta\lambda_o/2)\right]\cos(2\pi\zeta)d\zeta\,, \tag{34}$$

with ν the relative fluctuations in the index of refraction. Thus, the mean reflected power scales with the spectrum of the medium fluctuations at the scale of half the wavelength. The reflected power in our configuration is then maximized by tuning the wavelength to the correlation radius of the medium fluctuations in the longitudinal, z, direction.

4. **Mean reflected intensity.** In Appendix B we analyze the system (27) for $\mathcal{D}$ in the limit case $\alpha \to \infty$. This result allows us to get closed-form expressions for physically relevant quantities. In this section we consider the mean reflected intensity defined by

$$I^\varepsilon(\boldsymbol{x}) = \big\langle \mathbb{E}[|\check{a}^\varepsilon(\boldsymbol{x},0)|^2] \big\rangle \,. \tag{35}$$

Proposition 3. *As $\varepsilon \to 0$ and in the weak backscattering regime (21) the mean reflected intensity $I^\varepsilon(\boldsymbol{x})$ converges to $I(\boldsymbol{x})$ where*

$$I(\boldsymbol{x}) = \frac{1}{(2\pi)^{2d}} \iiint \Big\langle \hat{b}_0(\boldsymbol{k}_0')\overline{\hat{b}_0}(\boldsymbol{k}_1') \Big\rangle \, e^{i(\boldsymbol{k}_0'-\boldsymbol{k}_1')\cdot\boldsymbol{x}} D_{\boldsymbol{k}_0',\boldsymbol{k}_1',\boldsymbol{k}}(0)\, d\boldsymbol{k} d\boldsymbol{k}_0' d\boldsymbol{k}_1' \,. \tag{36}$$

This can also be written as

$$I(\boldsymbol{x}) = \frac{P_{\rm tot}}{\ell_x^d} \mathcal{I}\Big(\frac{\boldsymbol{x}}{\ell_x}\Big) \,, \tag{37}$$

with $P_{\rm tot}$ the mean reflected power given by (31).
If the source has covariance function

$$\Big\langle F(\boldsymbol{x}+\frac{\boldsymbol{y}}{2})\overline{F}(\boldsymbol{x}-\frac{\boldsymbol{y}}{2}) \Big\rangle = \exp\Big(-\frac{|\boldsymbol{x}|^2}{r_0^2} - \frac{|\boldsymbol{y}|^2}{4\rho_0^2}\Big) \,, \tag{38}$$

with a large radius $r_0 = \alpha \bar{r}_0$ and a large correlation radius $\rho_0 = \alpha\bar{\rho}_0$ (large means larger than ℓ_x), then the normalized intensity profile is independent of ρ_0 and with $L \gg L_{\rm att}$ it has the form:

$$\begin{aligned} \lim_{\alpha\to\infty} \alpha^d \mathcal{I}(\alpha \boldsymbol{y}) \quad &= \quad \frac{1}{(2\pi)^d} \int_0^\infty \int \exp\Big(-\frac{\bar{r}_0^2|\boldsymbol{s}|^2}{4\ell_x^2}\Big) \frac{\check{\mathcal{C}}_{K_z}(\boldsymbol{s}\zeta)}{\check{\mathcal{C}}_{K_z}(\boldsymbol{0})} \\ &\quad \times e^{\beta\int_0^{2\zeta} \check{\mathcal{C}}_0(\boldsymbol{s}\zeta') - \check{\mathcal{C}}_0(\boldsymbol{0}) d\zeta' - \zeta} e^{-i\boldsymbol{s}\cdot\boldsymbol{y}} d\boldsymbol{s} d\zeta \,. \end{aligned} \tag{39}$$

If the source has a large radius $r_0 = \alpha\bar{r}_0$ and a correlation radius ρ_0 of the order of or smaller than ℓ_x, then the normalized intensity profile depends on ρ_0 and for $L \gg L_{\rm att}$ it has the form:

$$\begin{aligned} \lim_{\alpha\to\infty} \alpha^d \mathcal{I}(\alpha \boldsymbol{y}) \quad &= \quad \frac{1}{(2\pi)^d} \int_0^\infty \int \exp\Big(-\frac{\bar{r}_0^2|\boldsymbol{s}|^2}{4\ell_x^2}\Big) \frac{\check{\mathcal{C}}_{K_z}(\boldsymbol{s}\zeta)}{\check{\mathcal{C}}_{K_z}(\boldsymbol{0})} \\ &\quad \times e^{\beta\int_0^{2\zeta} \check{\mathcal{C}}_0(\boldsymbol{s}\zeta') - \check{\mathcal{C}}_0(\boldsymbol{0}) d\zeta' - \zeta} \exp\Big(-\frac{|\boldsymbol{s}|^2\zeta^2\ell_x^2}{\rho_0^2}\Big) e^{-i\boldsymbol{s}\cdot\boldsymbol{y}} d\boldsymbol{s} d\zeta \,. \end{aligned} \tag{40}$$

This proposition gives information about the lateral spreading of the reflected wave field and how it depends on the correlation properties of the fluctuations of the random medium in a non-trivial way. The fact that the transverse profile of the reflected intensity depends in a non-trivial way of the medium statistics is good news from the inverse problem point of view. We discuss in Section 6.1 how the analytic expression of the transverse profile of the reflected intensity can be exploited for the estimation of medium statistics from the observation of the reflected intensity.

Proof. The mean reflected intensity is

$$I^\varepsilon(\boldsymbol{x}) = \frac{1}{(2\pi)^{2d}} \iiiint e^{i(\boldsymbol{k}_1-\boldsymbol{k}_2)\cdot\boldsymbol{x}} \mathbb{E}\big[\hat{\mathcal{R}}^\varepsilon(\boldsymbol{k}_1,\boldsymbol{k}_1',0)\overline{\hat{\mathcal{R}}^\varepsilon}(\boldsymbol{k}_2,\boldsymbol{k}_2',0)\big] \times \Big\langle \hat{b}_0(\boldsymbol{k}_1')\overline{\hat{b}_0}(\boldsymbol{k}_2')\Big\rangle \, d\boldsymbol{k}_1 d\boldsymbol{k}_1' d\boldsymbol{k}_2 d\boldsymbol{k}_2' \, .$$

By Proposition 1 we obtain that the limit of $I^\varepsilon(\boldsymbol{x})$ as $\varepsilon \to 0$ is (36). Using the dimensionless cross spectral density $\mathcal{D}$ (identity (25)) this can also be written as

$$I(\boldsymbol{x}) = \frac{\overline{D}_o \ell_x^{-3d}}{2^{3d}\pi^{2d}} \iiint \left\langle \hat{b}_0\left(\frac{\boldsymbol{v}+\boldsymbol{u}-\boldsymbol{w}}{2\ell_x}\right)\overline{\hat{b}_0}\left(\frac{\boldsymbol{v}-\boldsymbol{u}-\boldsymbol{w}}{2\ell_x}\right)\right\rangle \times e^{i\boldsymbol{u}\cdot\frac{\boldsymbol{x}}{\ell_x}} \mathcal{D}(\boldsymbol{u},\boldsymbol{v},\boldsymbol{w},0)\, d\boldsymbol{u}d\boldsymbol{v}d\boldsymbol{w} \, .$$

In the regime $\alpha \gg 1$, if the source is (38) with $r_0 = \alpha\bar{r}_0$, then by Lemma B.2 we obtain

$$\lim_{\alpha\to\infty} I(\alpha\boldsymbol{x}) = \frac{\overline{D}_o \bar{r}_0^d \rho_0^d}{2^{2d+2}\pi^d \ell_x^{3d}} \iiint \exp\Big(-\frac{\bar{r}_0^2|\boldsymbol{s}|^2}{4\ell_x^2} - \frac{\rho_0^2|\boldsymbol{v}-\boldsymbol{w}|^2}{4\ell_x^2}\Big) \times \mathcal{D}_{\boldsymbol{s}}(\boldsymbol{v},\boldsymbol{w},0) e^{i\boldsymbol{s}\cdot\frac{\boldsymbol{x}}{\ell_x}} d\boldsymbol{s}d\boldsymbol{v}d\boldsymbol{w} \, .$$

Substituting the expression (101) of $\mathcal{D}_{\boldsymbol{s}}(\boldsymbol{v},\boldsymbol{w},0)$ and integrating in $\boldsymbol{v}$ and $\boldsymbol{\lambda}$ gives (40), with

$$\frac{\overline{D}_o}{P_{\rm tot}} = \frac{\ell_x^d}{2^{d-2}\pi^{3d/2}\alpha^d \bar{r}_0^d}.$$

The result (39) follows similarly. □

In Section 6.1 we discuss in more detail the form of the reflected intensity in the case when the medium fluctuations are modeled in terms of a Matérn covariance function.

5. **Enhanced backscattering.** In this section, we give a mathematical proof of enhanced backscattering phenomenon and we compute the maximum, the angular width, and the shape of the enhanced backscattering cone. We also analyze the role of the spatial coherence of the source.

We consider the following experiment: for a given $\boldsymbol{k}_0$, we send a wave of unit amplitude, carrier transverse wavevector $\boldsymbol{k}_0$, radius $r_0 = \alpha\bar{r}_0$ and correlation radius $\rho_0 = \alpha\bar{\rho}_0$ into the medium. The covariance function of the source has the form:

$$\Big\langle F\big(\boldsymbol{x}+\frac{\boldsymbol{y}}{2}\big)\overline{F}\big(\boldsymbol{x}-\frac{\boldsymbol{y}}{2}\big)\Big\rangle = \exp\Big(-\frac{|\boldsymbol{x}|^2}{r_0^2} - \frac{|\boldsymbol{y}|^2}{4\rho_0^2} + i\boldsymbol{k}_0\cdot\boldsymbol{y}\Big) \, . \tag{41}$$

We record the reflected intensity in the backscattered direction $-\boldsymbol{k}_0$ or close to it. We observe as a function of relative transverse wavevector $\boldsymbol{k}$:

$$P^\varepsilon_{\boldsymbol{k},\boldsymbol{k}_0} := |\hat{a}^\varepsilon(-\boldsymbol{k}_0 + \alpha^{-1}\boldsymbol{k}, 0)|^2 \, , \tag{42}$$

which in view of the longitudinal (z-dependent) phase in Eq. (9) looks like a cone of angular aperture of order $\alpha^{-1}(\omega\ell_x/c_o)^{-1}$.

If we average with respect to the random medium and the source, and consider the asymptotic regime $\varepsilon \to 0$, then this means that we are interested in

$$P_{\boldsymbol{k},\boldsymbol{k}_0} = \lim_{\varepsilon\to 0} \big\langle \mathbb{E}\big[P^\varepsilon_{\boldsymbol{k},\boldsymbol{k}_0}\big]\big\rangle \, . \tag{43}$$

This is the mean intensity reflected by the random region $\mathbb{R}^d \times (-L, 0)$ in the backscattered direction (for $\boldsymbol{k} = \boldsymbol{0}$) or close to the backscattered direction, in a direction whose angle with respect to the backscattered direction is of order

$\alpha^{-1}(\omega\ell_x/c_o)^{-1}$ (for $\boldsymbol{k} \neq \mathbf{0}$). We also consider the $\boldsymbol{k}_0$-average of this quantity, that turns out to have a simple expression as shown in the following proposition:

$$P_{\boldsymbol{k}} = \int P_{\boldsymbol{k},\boldsymbol{k}_0} d\boldsymbol{k}_0 \,. \tag{44}$$

Proposition 4. *In the regime $\alpha \gg 1$ and $L \gg L_{\rm att}$ the mean intensity reflected in the direction $\boldsymbol{k}$ relative to the backscattered direction has the form*

$$\lim_{\alpha\to\infty} P_{\boldsymbol{k},\boldsymbol{k}_0} = P_{\rm tot}\mathcal{P}_{\boldsymbol{k}_0}(\boldsymbol{k})\,, \tag{45}$$

with $P_{\rm tot}$ the mean reflected power (33) and

$$\begin{aligned}\mathcal{P}_{\boldsymbol{k}_0}(\boldsymbol{k}) \;=\; & \ell_x^d \frac{\bar\rho_0^d}{\pi^{d/2}} \int d\boldsymbol{k}' \exp\big(-\bar\rho_0^2|\boldsymbol{k}'|^2\big)\Big\{ \int d\boldsymbol{\lambda} \frac{\check{\mathcal{C}}_{K_z}(\boldsymbol{\lambda})}{\check{\mathcal{C}}_{K_z}(\mathbf{0})} e^{i2\boldsymbol{\lambda}\cdot\boldsymbol{k}_0\ell_x} \\ & \times\Big[\int_0^\infty e^{\beta\int_0^\zeta \check{\mathcal{C}}_0(\boldsymbol{\lambda}+(\boldsymbol{k}-\boldsymbol{k}')\ell_x\zeta')+\check{\mathcal{C}}_0(\boldsymbol{\lambda}-(\boldsymbol{k}-\boldsymbol{k}')\ell_x\zeta')-2\check{\mathcal{C}}_0(\mathbf{0})d\zeta'-\zeta} d\zeta \\ & + \frac{1}{1+2\beta(\check{\mathcal{C}}_0(\mathbf{0})-\check{\mathcal{C}}_0(\boldsymbol{\lambda}))} - \frac{1}{1+2\beta\check{\mathcal{C}}_0(\mathbf{0})}\Big]\Big\}\,. \end{aligned} \tag{46}$$

The $\boldsymbol{k}_0$-average (44) of the the mean reflected intensity has the form

$$\lim_{\alpha\to\infty} P_{\boldsymbol{k}} = \pi^d P_{\rm tot}\mathcal{P}(\boldsymbol{k})\,, \tag{47}$$

with

$$\begin{aligned}\mathcal{P}(\boldsymbol{k}) = \frac{\bar\rho_0^d}{\pi^{d/2}} \int d\boldsymbol{k}' \exp\big(-\bar\rho_0^2|\boldsymbol{k}'|^2\big)\Big\{ \int_0^\infty e^{2\beta\int_0^\zeta \check{\mathcal{C}}_0((\boldsymbol{k}-\boldsymbol{k}')\ell_x\zeta')-\check{\mathcal{C}}_0(\mathbf{0})d\zeta'-\zeta} d\zeta \\ + \frac{2\beta\check{\mathcal{C}}_0(\mathbf{0})}{1+2\beta\check{\mathcal{C}}_0(\mathbf{0})}\Big\}\,. \end{aligned} \tag{48}$$

Proof. We have

$$P^\varepsilon_{\boldsymbol{k},\boldsymbol{k}_0} = \Big|\int \hat{\mathcal{R}}^\varepsilon(-\boldsymbol{k}_0+\alpha^{-1}\boldsymbol{k},\boldsymbol{k}',0)\hat{b}_0(\boldsymbol{k}')\,d\boldsymbol{k}'\Big|^2\,,$$

and therefore

$$P_{\boldsymbol{k},\boldsymbol{k}_0} = \frac{(2\pi\alpha\bar r_0\bar\rho_0)^d}{4}\int D_{\boldsymbol{k}_0+\alpha^{-1}\boldsymbol{k}',\boldsymbol{k}_0+\alpha^{-1}\boldsymbol{k}',-2\boldsymbol{k}_0+\alpha^{-1}(\boldsymbol{k}-\boldsymbol{k}')}(0)\exp\big(-\bar\rho_0^2|\boldsymbol{k}'|^2\big)\,d\boldsymbol{k}'\,.$$

When $\alpha \gg 1$ we find by Lemma B.2 that the mean reflected intensity observed in the relative direction $\boldsymbol{k}$ is

$$\lim_{\alpha\to\infty}\alpha^{-d}P_{\boldsymbol{k},\boldsymbol{k}_0} = \frac{(2\pi\bar r_0\bar\rho_0)^d\overline{D}_o}{4}\int \mathcal{D}_{(\boldsymbol{k}'+\boldsymbol{k})\ell_x,\mathbf{0}}(-2\boldsymbol{k}_0\ell_x,0)\exp\big(-\bar\rho_0^2|\boldsymbol{k}'|^2\big)d\boldsymbol{k}'\,.$$

By substituting the expressions (98) and (101-102) in this equation, we get the desired result. □

When the source is a plane wave (i.e. $\bar r_0 \to \infty$) fully coherent (i.e. $\bar\rho_0 \to \infty$), then $\mathcal{P}(\boldsymbol{k})$ has the form

$$\mathcal{P}_{\rm P}(\boldsymbol{k}) = \int_0^\infty e^{2\beta\int_0^\zeta \check{\mathcal{C}}_0(\boldsymbol{k}\ell_x\zeta')-\check{\mathcal{C}}_0(\mathbf{0})d\zeta'-\zeta}d\zeta + \frac{2\beta\check{\mathcal{C}}_0(\mathbf{0})}{1+2\beta\check{\mathcal{C}}_0(\mathbf{0})}\,. \tag{49}$$

The partial coherence introduces a smoothing of the cone, in the sense that the cone (48) is the convolution of the perfect cone (49) with the covariance function of the source:

$$\mathcal{P}(\boldsymbol{k}) = \frac{\bar{\rho}_0^d}{\pi^{d/2}} \int d\boldsymbol{k}' \exp\big(-\bar{\rho}_0^2 |\boldsymbol{k}'|^2\big) \mathcal{P}_{\rm P}(\boldsymbol{k}-\boldsymbol{k}'). \tag{50}$$

The mean reflected intensity in an arbitrary direction out of the small cone around the backscattered direction can be obtained by taking the limit $|\boldsymbol{k}| \to \infty$:

$$\lim_{|\boldsymbol{k}|\to\infty} \mathcal{P}_{\rm P}(\boldsymbol{k}) = 1\,. \tag{51}$$

The maximum of the enhanced backscattering cone is reached at $\boldsymbol{k}=\boldsymbol{0}$ for an incident plane wave, that is, for the exact backscattered direction, and this maximum is given by

$$\max_{\boldsymbol{k}\in\mathbb{R}^d} \mathcal{P}_{\rm P}(\boldsymbol{k}) = \mathcal{P}_{\rm P}(\boldsymbol{0}) = \frac{1+4\beta\check{\mathcal{C}}_0(\boldsymbol{0})}{1+2\beta\check{\mathcal{C}}_0(\boldsymbol{0})}\,, \tag{52}$$

which takes values in the interval $(1,2)$. In the weak forward-scattering regime $\beta \ll 1$, the enhancement factor is equal to 1. In the strong forward-scattering regime $\beta \gg 1$, the enhancement factor is equal to 2. In Section 6.2 we discuss the structure of the cone in more detail in the case that the medium fluctuations are modeled in terms of the Matérn covariance function.

We remark that above we averaged with respect to the random medium and the source when we computed the cone structure. The averaging with respect to the source is obtained in practice by the use of partially coherent sources, which are realizations of a source with covariance structure (41) that ergodically fluctuates in time. A photodetector integrates in time the different realizations hence the averaging with respect to the source distribution. The averaging with respect to the medium is, however, a critical issue. In practice the statistical stability of the cone is an important aspect and without proper averaging the cone may be buried in speckle noise. This stability can be achieved as we have proposed in Eq. (44), by averaging with respect to the incident angle. In biological applications the incidence angle is usually fixed but partially coherent sources have been exploited as an important technique to enhance statistical stability, essentially by providing independent views of the medium via the structure in the source, however, at the cost of blurring of the cone as seen in Eq. (50). Motivated by applications Low-Coherence-Enhanced-BackScattering (LEBS) [22, 21, 34] systems have been designed that elegantly achieve statistical stability via partially coherent sources. In fact, both approaches (averaging with respect to the incidence angle or by the use of partially coherent sources) for signal enhancement can be expressed as averaging with respect to transverse wavevector. This is clear for the average with respect to the incidence angle, and, if we take into account the ergodic average with respect to the source distribution (17):

$$\big\langle |\hat{a}^\varepsilon(-\boldsymbol{k}_0+\boldsymbol{k})|^2 \big\rangle = \frac{(4\pi\rho_0 r_0)^d}{4} \iint \hat{\mathcal{R}}^\varepsilon(-\boldsymbol{k}_0+\boldsymbol{k}, \boldsymbol{k}_1+\boldsymbol{k}_2+\boldsymbol{k}_0)$$
$$\times \overline{\hat{\mathcal{R}}^\varepsilon}(-\boldsymbol{k}_0+\boldsymbol{k}, \boldsymbol{k}_1-\boldsymbol{k}_2+\boldsymbol{k}_0) \exp\big(-r_0^2|\boldsymbol{k}_2|^2 - \rho_0^2|\boldsymbol{k}_1|^2\big) d\boldsymbol{k}_1 d\boldsymbol{k}_2\,, \tag{53}$$

then we observe that a small ρ_0 gives averaging with respect to $\boldsymbol{k}_1$. Thus, decorrelation in the reflection coefficient with respect to transverse wavevector gives enhanced signal-to-noise ratio. We expect that the averaging with respect to $\boldsymbol{k}_0$, and/or $\boldsymbol{k}_1$ as in LEBS, is sufficient to ensure the averaging with respect to the random medium

fluctuations, a detailed proof of this self-averaging property would require to study higher-order moments as in [15], which is beyond the scope of this paper. We can summarize by saying that reducing the coherence of the illumulation (i.e. reducing ρ_0) increases the signal-to-noise ratio but also smoothes the enhanced backscattering cone. This is a traditional trade-off between resolution and stability.

6. **Backscattering characteristics for Matérn covariance function.** In biological applications appropriate modeling of the tissue fabric is important both from the point of view of techniques that use scattering for diagnostic information as well as for proper dose distribution in therapies involving focused beams, while in atmospheric propagation proper modeling is critical in the design of imaging and communication systems. Here we will consider a specific model for the covariance function of the medium fluctuations, the commonly used Matérn covariance function or family. Tissue modeling with the Matérn covariance function is nicely reviewed in [29]. Here we will model the covariance function of the medium fluctuations as

$$\int \mathbb{E}[\nu(\boldsymbol{x}'+\boldsymbol{x},z'+z)\nu(\boldsymbol{x}',z')]dz = \sigma^2\ell_z\check{\mathcal{C}}_0\Big(\frac{\boldsymbol{x}}{\ell_x}\Big)\,, \tag{54}$$

with

$$\check{\mathcal{C}}_0(\boldsymbol{s}) = \mathcal{M}_p(\boldsymbol{s}) := \frac{\big(2\sqrt{p}|\boldsymbol{s}|\big)^p}{\Gamma(p)2^{p-1}}K_p\left(2\sqrt{p}|\boldsymbol{s}|\right)\,, \tag{55}$$

for K_p the modified Bessel function of the second kind of order p. Note that we assume that the dimension $d = 2$ throughout this section. The parameter $p \in [1/2,\infty)$ characterizes the smoothness of the process with larger values for p giving a smoother process. We remark that the notation $D = 2p+2$ is sometimes used for the spectral exponent. Some important special cases for the Matérn covariance function are:

$$\lim_{p\to\infty}\mathcal{M}_p(\boldsymbol{s}) \;=\; \exp(-|\boldsymbol{s}|^2)\,,\quad \text{Gaussian}\,, \tag{56}$$

$$\mathcal{M}_{1/2}(\boldsymbol{s}) \;=\; \exp(-\sqrt{2}|\boldsymbol{s}|)\,,\quad \text{Exponential}\,. \tag{57}$$

The case $p = 5/6$ corresponds to the von Kármán spectrum of Kolmogorov turbulence with zero inner scale and outer scale L_0 and associated with the spectrum:

$$\iint \mathbb{E}[\nu(\boldsymbol{x}'+\boldsymbol{x},z'+z)\nu(\boldsymbol{x}',z')]e^{-i\boldsymbol{k}\cdot\boldsymbol{x}}dzd\boldsymbol{x} = 0.033C_n^2\Big(\frac{1}{L_0^2}+|\boldsymbol{k}|^2\Big)^{-11/6}, \tag{58}$$

where $L_0 = \ell_x/(2\sqrt{p})$ and $0.033C_n^2 = 4\pi p\sigma^2 L_0^{-2p}$. We have the asymptotics

$$\mathcal{M}_p(\boldsymbol{s}) = 1 - \frac{p^p\Gamma(1-p)}{\Gamma(1+p)}|\boldsymbol{s}|^{2p} + o(|\boldsymbol{s}|^{2p}) \quad \text{as} \quad |\boldsymbol{s}|\to 0^+, \tag{59}$$

for $1/2 \le p < 1$. We remark that in the Kolmogorov case this corresponds to a structure function with the growth $|\boldsymbol{s}|^{5/3}$ (rather than the Kolmogorov structure function growth of $|\boldsymbol{s}|^{2/3}$), which is a consequence of the fact that we integrated the covariance function of the medium fluctuations in the z dimension.

In [27, 33] it is discussed how the medium parameters, essentially $\{p,\sigma^2\ell_z,\ell_x\}$, relate to the optical scattering parameters and in turn how these relate to the shape of the cone, moreover, how the cone shape parameters can then be used to construct a LEBS Marker for early indication of cancerous tissue. The connection between medium parameters and the cone is in this analysis partly based on empirical equations derived from Monte-Carlo simulations and assumes weak backscattering modeled in terms of a Born approximation [4, 28]. Here, we consider a regime of stronger

multiple scattering effects in the context of the scaling regime outlined above. Our analysis can be used to link the medium parameters to the shape of the cone. In our modeling we incorporate the effects of random forward as well as lateral scattering. We give next some asymptotic forms for the mean reflected intensity profile and the enhanced backscattering cone in the regime $\beta \gg 1$ corresponding to strong forward scattering.

6.1. **Reflected intensity profile.** The profile of the mean reflected intensity is described in Proposition 3. Here we want to focus on the physically relevant case, when the initial beam has a large coherence radius $\rho_0 \gg \ell_x$ and a large beam radius such that $r_0 \gg \ell_x$ but $r_0 \ll \lambda_o L_{\rm att}/\ell_x$. The last condition means that the radius of the mean reflected intensity is determined by scattering and not by the initial beam radius (equivalently, the initial beam radius is negligible compared to the beam spreading due to scattering). This means that we deal with Eq. (38) with $\rho_0 = \alpha\bar\rho_0$, $r_0 = \alpha\bar r_0$, and $\bar r_0 \ll \ell_x$. Then we get from (39) that the mean reflected intensity is

$$\lim_{\alpha\to\infty} \alpha^2 \mathcal{I}(\alpha \boldsymbol{y}) = \frac{1}{(2\pi)^2} \int_0^\infty \int \frac{\check{\mathcal{C}}_{K_z}(\boldsymbol{s}\zeta)}{\check{\mathcal{C}}_{K_z}(\boldsymbol{0})} e^{\beta \int_0^{2\zeta} \check{\mathcal{C}}_0(\boldsymbol{s}\zeta') - \check{\mathcal{C}}_0(\boldsymbol{0}) d\zeta' - \zeta} e^{-i\boldsymbol{s}\cdot\boldsymbol{y}} d\boldsymbol{s} d\zeta \,, \quad (60)$$

which is independent of $\bar\rho_0$ and $\bar r_0$. We aim at showing that this expression becomes simple when forward scattering is strong $\beta \gg 1$, which requires us to distinguish the cases in which $\check{\mathcal{C}}_0$ is smooth or not at $\boldsymbol{0}$.

Let us first consider the smooth case with $\check{\mathcal{C}}_0(\boldsymbol{s}) = \mathcal{M}_\infty(\boldsymbol{s})$. Then we can make use of the expansion $\check{\mathcal{C}}_0(\boldsymbol{s}) \simeq 1 - |\boldsymbol{s}|^2 + o(|\boldsymbol{s}|^2)$ as $|\boldsymbol{s}| \to 0$. Since we can anticipate from (60) that the radius of the mean reflected intensity is of order $\alpha\beta^{1/2}\ell_x$, we look at the mean intensity profile at this particular scale and we obtain using Proposition 3:

$$\lim_{\beta\to\infty} \lim_{\alpha\to\infty} \alpha^2 \beta \mathcal{I}(\alpha\beta^{1/2}\boldsymbol{y}) = \mathcal{Q}_\infty(\boldsymbol{y}) \,, \quad (61)$$

where

$$\mathcal{Q}_\infty(\boldsymbol{y}) = \frac{1}{4\pi} \int_0^\infty e^{-\frac{|\boldsymbol{y}|^2}{4}\frac{3}{8\zeta^3}} \Big(\frac{3}{8\zeta^3}\Big) e^{-\zeta} \, d\zeta \,. \quad (62)$$

The dimensionless intensity profile $\mathcal{Q}_\infty(\boldsymbol{y})$ is normalized so that $\int \mathcal{Q}_\infty(\boldsymbol{y}) d\boldsymbol{y} = 1$. Therefore the asymptotic expressions satisfy $\int \mathcal{I}(\boldsymbol{y}) d\boldsymbol{y} = 1$ and $\int I(\boldsymbol{x}) d\boldsymbol{x} = P_{\rm tot}$. The mean intensity profile has sub-exponential decay for large $|\boldsymbol{y}|$,

$$\mathcal{Q}_\infty(\boldsymbol{y}) \propto |\boldsymbol{y}|^{-5/4} \exp\big(-\sqrt{|\boldsymbol{y}|} 2^{3/4}/\sqrt{3}\big) \text{ for } |\boldsymbol{y}| \gg 1, \quad (63)$$

given by the contributions of the waves that have propagated deep into the medium. It also has power divergence for small $|\boldsymbol{y}|$,

$$\mathcal{Q}_\infty(\boldsymbol{y}) \propto |\boldsymbol{y}|^{-4/3} \text{ for } |\boldsymbol{y}| \ll 1. \quad (64)$$

This is given by the contributions of reflections that occur close to the surface $z = 0$. The radius ℓ_∞ of the mean intensity profile is

$$\ell_\infty = \ell_x \alpha \beta^{1/2} = \sqrt{\sigma^2 \ell_z L_{\rm att}} \left(\frac{L_{\rm att}}{2\ell_x}\right). \quad (65)$$

Thus, the spreading is independent of the wavelength and is stronger when the attenuation distance is larger so that the wave propagates deeper into the medium, moreover, is stronger with a larger longitudinal correlation length $\sigma^2\ell_z$. Note, however, that the spreading is inversely proportional to the lateral coherence length ℓ_x so that smooth transverse medium variations give less spreading.

Let us next consider the case in which $\check{\mathcal{C}}_0(\boldsymbol{s})$ is not smooth at $\mathbf{0}$ and has the form $\check{\mathcal{C}}_0(\boldsymbol{s}) = 1 - c_p|\boldsymbol{s}|^{2p} + o(|\boldsymbol{s}|^{2p})$, with

$$c_p = p^p\Gamma(1-p)/\Gamma(1+p)\,, \tag{66}$$

for $1/2 \le p < 1$. This corresponds to a rough random medium, with jumps in the derivative of ν. We then find that

$$\lim_{\beta\to\infty}\lim_{\alpha\to\infty} \alpha^2\beta^{1/p}\mathcal{I}(\alpha\beta^{1/(2p)}\boldsymbol{y}) \quad = \quad \mathcal{Q}_p(\boldsymbol{y})\,, \tag{67}$$

where

$$\mathcal{Q}_p(\boldsymbol{y}) = \frac{1}{(2\pi)^2}\int\int_0^\infty e^{-\frac{c_p 2^{p+1}\zeta^{2p+1}|\boldsymbol{s}|^{2p}}{2p+1}-\zeta}e^{-i\boldsymbol{s}\cdot\boldsymbol{y}}d\zeta d\boldsymbol{s}. \tag{68}$$

Thus, in this case the radius ℓ_p of the mean intensity profile is

$$\ell_p = \ell_x\alpha\beta^{1/(2p)} = \Big(\sigma^2\ell_z L_{\rm att}\Big)^{1/(2p)}\Big(\frac{L_{\rm att}}{2\ell_x}\Big)\Big(\frac{\pi}{\lambda_o}\Big)^{(1-p)/p}. \tag{69}$$

This shows that, when medium variations are rough, then the intensity spreading is more sensitive to the correlation length, moreover, it actually depends on the wavelength λ_o at a fractional power with a smaller wavelength and rougher medium giving stronger spreading. Note that we also obtain in this rough case a power law decay at infinity and a power divergence at $\mathbf{0}$:

$$\mathcal{Q}_p(\boldsymbol{y}) \propto |\boldsymbol{y}|^{-(2p+2)/(2p+1)} \text{ for } |\boldsymbol{y}| \ll 1\,, \tag{70}$$

$$\mathcal{Q}_p(\boldsymbol{y}) \propto |\boldsymbol{y}|^{-2p-2} \text{ for } |\boldsymbol{y}| \gg 1\,. \tag{71}$$

In order to establish the last result we have used the fact that the two-dimensional Fourier transform of $\exp(-|\boldsymbol{s}|^{2p})$ decays as $|\boldsymbol{y}|^{-2p-2}$; this has been studied in the literature because it is the density of a multivariate stable distribution [26].

The special case $p = 1/2$ corresponds to the exponential correlation function in Eq. (57). We remark that in this case we get

$$\mathcal{Q}_{1/2}(\boldsymbol{y}) = \frac{1}{\pi}\int_0^\infty \frac{\zeta^2 e^{-\zeta}}{(|\boldsymbol{y}|^2+4\zeta^4)^{3/2}}d\zeta\,, \tag{72}$$

which again is such that $\int \mathcal{Q}_{1/2}(\boldsymbol{y})d\boldsymbol{y} = 1$. The radius of the mean intensity profile is of order $\alpha\beta\ell_x \propto 1/\lambda_o$ and it decays as $|\boldsymbol{y}|^{-3}$ at infinity and it diverges as $|\boldsymbol{y}|^{-3/2}$ at zero. This can be contrasted with the result obtained in the case of a smooth random medium, where the beam has sub-exponential tail at infinity and a width of order $\alpha\beta^{1/2}\ell_x$ independent of λ_0.

6.2. **Enhanced backscattering cone.** The shape $\mathcal{P}_{\rm P}(\boldsymbol{k})$ of the perfect cone is given by (49) for any value of β. We can give a more quantitative description in the regime $\beta \gg 1$, but this analysis requires us to distinguish the cases in which $\check{\mathcal{C}}_0$ is smooth or not at $\mathbf{0}$.

Let us first consider the smooth case with $\check{\mathcal{C}}_0(\boldsymbol{s}) = \mathcal{M}_\infty(\boldsymbol{s})$. In this case we can expand as $\check{\mathcal{C}}_0(\boldsymbol{s}) \simeq 1 - |\boldsymbol{s}|^2 + o(|\boldsymbol{s}|^2)$ and we find that

$$\lim_{\beta\to\infty}\mathcal{P}_{\rm P}(\beta^{-1/2}\boldsymbol{k}) = \mathcal{Q}_{{\rm EBC},\infty}(\boldsymbol{k}\ell_x), \qquad \mathcal{Q}_{{\rm EBC},\infty}(\boldsymbol{s}) = 1+\int_0^\infty e^{-\frac{2\zeta^3}{3}|\boldsymbol{s}|^2-\zeta}\,d\zeta\,. \tag{73}$$

For small $|\boldsymbol{s}|$, we have

$$\mathcal{Q}_{{\rm EBC},\infty}(\boldsymbol{s}) = 2 - 4|\boldsymbol{s}|^2 + o(|\boldsymbol{s}|^2), \tag{74}$$

which shows that the peak is smooth. For large $|\boldsymbol{s}|$, we obtain

$$\mathcal{Q}_{\mathrm{EBC},\infty}(\boldsymbol{s}) = 1 + 18^{-1/3}\Gamma(1/3)|\boldsymbol{s}|^{-2/3} + o(|\boldsymbol{s}|^{-2/3})\,, \tag{75}$$

which shows that the angular aperture of the enhanced backscattering cone is of order (taking into account (65)):

$$A_{\mathrm{EBC}} = \frac{\lambda_o}{\ell_x \alpha \beta^{1/2}} = \frac{\lambda_o}{\ell_\infty}\,. \tag{76}$$

In particular this means that the cone width is proportional to the wavelength λ_o.

Let us next consider the case in which $\check{\mathcal{C}}_0(\boldsymbol{s})$ is not smooth at $\mathbf{0}$ and has the form $\check{\mathcal{C}}_0(\boldsymbol{s}) = 1 - c_p|\boldsymbol{s}|^{2p} + o(|\boldsymbol{s}|^{2p})$, with $c_p = p^p\Gamma(1-p)/\Gamma(1+p)$ and $1/2 \le p < 1$. We find that

$$\lim_{\beta\to\infty} \mathcal{P}_{\mathrm{P}}(\beta^{-1/2p}\boldsymbol{k}) = \mathcal{Q}_{\mathrm{EBC},p}(\boldsymbol{k}\ell_x)\,, \qquad \mathcal{Q}_{\mathrm{EBC},p}(\boldsymbol{s}) = 1 + \int_0^\infty e^{-\frac{2c_p\zeta^{2p+1}|\boldsymbol{s}|^{2p}}{2p+1} - \zeta}\, d\zeta\,. \tag{77}$$

This shows that the angular aperture of the enhanced backscattering cone is now of order (taking into account (69)):

$$A_{\mathrm{EBC}} = \frac{\lambda_o}{\ell_x \alpha \beta^{1/(2p)}} = \frac{\lambda_o}{\ell_p}\,.$$

In particular this means that the cone width is proportional to the wavelength λ_o to a fractional power: $\lambda_o^{2-1/p}$.

For small $|\boldsymbol{s}|$ we have

$$\mathcal{Q}_{\mathrm{EBC},p}(\boldsymbol{s}) = 2 - 2c_p\Gamma(2p+1)|\boldsymbol{s}|^{2p} + o(|\boldsymbol{s}|^{2p})\,, \tag{78}$$

which shows that the peak is not smooth but has a cusp. For large $|\boldsymbol{s}|$, we obtain

$$\mathcal{Q}_{\mathrm{EBC},p}(\boldsymbol{s}) = 1 + \frac{\Gamma(1/(2p+1))}{(2p+1)^{2p/(2p+1)}(2c_p)^{1/(2p+1)}}|\boldsymbol{s}|^{-2p/(2p+1)} + o(|\boldsymbol{s}|^{-2p/(2p+1)})\,. \tag{79}$$

To summarize, for both smooth and rough media, we have obtained that the radius ℓ of the mean reflected intensity and the angular aperture A_{EBC} of the enhanced backscattering cone are related to each other through the duality relation:

$$A_{\mathrm{EBC}} \sim \frac{\lambda_o}{\ell}\,. \tag{80}$$

This relation is in agreement with the physical interpretation of enhanced backscattering as a constructive interference between pairs of wave "paths" and reversed paths, see Figure 1. If the reflected wave is observed with an angle A compared to the backscattered direction, then the phase shift between the direct and reversed paths is $\omega e/c_o = \omega d \sin A/c_o$, where d is the typical transverse size of a wave path, which is in our setting of the order of the radius ℓ of the reflected intensity. Therefore, constructive interference is possible if $\omega\ell A/c_o \le 1$, which gives the angular aperture of the enhanced backscattering cone. This "path" interpretation is not used in our paper, but we recover the physical result by exploiting our characterization of the second-order moments of the reflection operator.

7. **Summary and medium parameter estimation.** In a typical experimental configuration one can measure the profile and the radius of the backscattered intensity in the near field $|\check{a}^\varepsilon(\boldsymbol{x},0)|^2$ and/or in the far field $|\hat{a}^\varepsilon(\boldsymbol{k},0)|^2$, with the latter corresponding to enhanced backscattering type of data. The analysis presented in this paper shows that the two sets of observations provide the same information. The shapes of the profiles, with either near or far field data, make it possible to identify the smoothness of the medium. The magnitudes and radii of the profiles make it possible to identify parameters that are combinations of the statistics of the random medium (standard deviation and the correlation radii) and of the attenuation of the medium. The estimation of these parameters can help to classify biological tissue in medical imaging and the state of the atmosphere in atmospheric propagation. We remark that in practice, far field measurements are usually easier than near field measurements.

We next summarize our results and review more specifically how the profile parameters relate to the medium model. We have considered a time-harmonic high-frequency regime with rapid anisotropic medium fluctuations on the microscale as described by Eqs. (1) and (2) with $\varepsilon \ll 1$. We assume a regime of weak backscattering as described by (21), moreover, a random half-space or a random region with thickness $L \gg L_{\rm att}$ and a large inverse Fresnel number

$$\alpha = \frac{\lambda_o L_{\rm att}}{2\pi \ell_x^2} \gg 1\,,$$

for λ_o the wavelength, ℓ_x the lateral correlation radius of the medium fluctuations, and $L_{\rm att}$ the attenuation length. Then we find that the mean intensity profile is described by Proposition 3 and the enhanced backscattering cone is described by Proposition 4. This is the main regime and also the main results of our paper.

In order to get more qualitative insight about how the profiles depend on the medium fabric we consider next some subsequent scaling relations.
Consider the case with large beam and coherence radii for the partly coherent source as described by Eq. (38) with $\alpha\ell_x \gg r_0 \geq \rho_0 \gg \ell_x$. Then we find the simplified expressions for the near field mean intensity measurements at the surface of the complex halfspace:

$$\big\langle \mathbb{E}[|\check{a}^\varepsilon(\boldsymbol{x},0)|^2]\big\rangle = \frac{P_{\rm tot}}{(2\pi\ell_x\alpha)^2}\int_0^\infty \int \frac{\check{\mathcal{C}}_{K_z}(\boldsymbol{s}\zeta)}{\check{\mathcal{C}}_{K_z}(\boldsymbol{0})} e^{\beta\int_0^{2\zeta}\check{\mathcal{C}}_0(\boldsymbol{s}\zeta')-\check{\mathcal{C}}_0(\boldsymbol{0})d\zeta'-\zeta} e^{-i\boldsymbol{s}\cdot\boldsymbol{x}/(\alpha\ell_x)} d\boldsymbol{s}d\zeta\,,$$

with $P_{\rm tot}$ the mean reflected power given by (32) and $\check{\mathcal{C}}_{K_z}$ a partial Fourier transform of the medium fluctuations, see Eqs. (23) and (28).
Consider the case with large beam and coherence radii for the partly coherent source as described by Eq. (41) with $\alpha\ell_x \gg \rho_0 \gg \ell_x$ and $\boldsymbol{k}_0$ the transverse wavevector corresponding to the probing direction. Then we find the simplified expressions for the far field measurements:

$$\begin{aligned}
&\big\langle \mathbb{E}\big[|\hat{a}^\varepsilon(-\boldsymbol{k}_0+\boldsymbol{k},0)|^2\big]\big\rangle \\
&= \ell_x^2 P_{\rm tot}\int \frac{\check{\mathcal{C}}_{K_z}(\boldsymbol{\lambda})}{\check{\mathcal{C}}_{K_z}(\boldsymbol{0})} e^{i2\boldsymbol{\lambda}\cdot\boldsymbol{k}_0\ell_x}\Big[\int_0^\infty e^{\beta\int_0^\zeta \check{\mathcal{C}}_0(\boldsymbol{\lambda}+\boldsymbol{k}\alpha\ell_x\zeta')+\check{\mathcal{C}}_0(\boldsymbol{\lambda}-\boldsymbol{k}\alpha\ell_x\zeta')-2\check{\mathcal{C}}_0(\boldsymbol{0})d\zeta'-\zeta} d\zeta \\
&\qquad + \frac{1}{1+2\beta(\check{\mathcal{C}}_0(\boldsymbol{0})-\check{\mathcal{C}}_0(\boldsymbol{\lambda}))} - \frac{1}{1+2\beta\check{\mathcal{C}}_0(\boldsymbol{0})}\Big] d\boldsymbol{\lambda}\,,
\end{aligned}$$

and for the far field measurements averaged over incoming direction we have

$$\int \left\langle \mathbb{E}\big[|\hat{a}^\varepsilon(-\boldsymbol{k}_0+\boldsymbol{k},0)|^2\big]\right\rangle d\boldsymbol{k}_0 \\ = \pi^2 P_{\rm tot}\left(\int_0^\infty e^{2\beta\int_0^\zeta \check{\mathcal{C}}_0(\zeta'\boldsymbol{k}\alpha\ell_x)-\check{\mathcal{C}}_0(\boldsymbol{0})d\zeta'-\zeta}d\zeta + \frac{2\beta\check{\mathcal{C}}_0(\boldsymbol{0})}{1+2\beta\check{\mathcal{C}}_0(\boldsymbol{0})}\right). \quad (81)$$

In Figure 2 we show the enhancement profile (81) (normalized by $\pi^2 P_{\rm tot}$). Here we use the Matérn covariance function (55). Note that a larger p and smoother medium fluctuations give a broader backscattering enhancement cone and that a large value for β gives a sharp cusp like cone with a maximum enhancement factor of two. In-

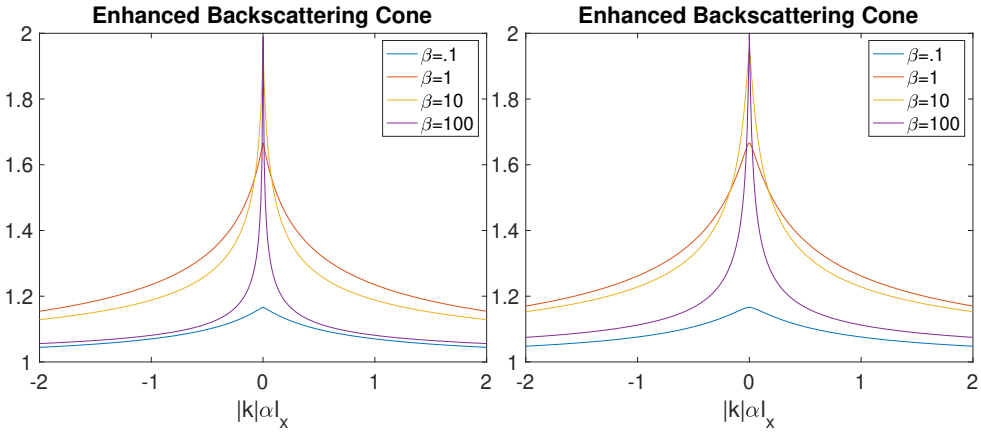

FIGURE 2. The backscattering enhancement cone in Eq. (81) (normalized by $\pi^2 P_{\rm tot}$). Here we use the Matérn covariance function (55). In the left plot $p = .6$, while in the right plot $p = .9$ so that the medium fluctuations are smoother in the right plot. In the plots the narrowest cones with largest peak values correspond to the largest β values.

deed, a broad support in near field intensity measurements corresponds to a narrow far field enhanced backscattering cone. Moreover, rough medium fluctuations give wavelength-dependent intensity profiles.

In order to get more insight about how the profiles depend on the medium fabric and articulate the main parameters that can be identified we consider finally the regime of strong forward scattering:

$$\beta = \frac{\pi^2\sigma^2\ell_z L_{\rm att}}{\lambda_o^2} \gg 1\,,$$

for ℓ_z the correlation radius in the longitudinal direction and σ the standard deviation of the medium fluctuations. Moreover, we model the medium fluctuations in terms of the Matérn correlation function (55). Then we find that the intensity profile has the principal shape

$$\left\langle \mathbb{E}[|\check{a}^\varepsilon(\boldsymbol{x},0)|^2]\right\rangle \quad = \quad \frac{P_{\rm tot}}{\ell_p^2}\mathcal{Q}_p\Big(\frac{\boldsymbol{x}}{\ell_p}\Big)\,, \quad (82)$$

with

$$\mathcal{Q}_p\left(\boldsymbol{y}\right) \propto \left\{ \begin{array}{ll} |\boldsymbol{y}|^{-(2p+2)/(2p+1)} & \text{for } |\boldsymbol{y}| \ll 1\,, \\ |\boldsymbol{y}|^{-2p-2} & \text{for } |\boldsymbol{y}| \gg 1\,. \end{array} \right.$$

We also find that the enhanced backscattering cone averaged over incoming direction has the principal shape

$$\int \left\langle \mathbb{E}\big[|\hat{a}^\varepsilon(-\boldsymbol{k}_0+\boldsymbol{k},0)|^2\big]\right\rangle d\boldsymbol{k}_0 \quad = \quad \pi^2 P_{\rm tot}\,\mathcal{Q}_{{\rm EBC},p}\left(\boldsymbol{k}\ell_p\right)\,, \tag{83}$$

with

$$\mathcal{Q}_{{\rm EBC},p}\left(\boldsymbol{s}\right) \simeq \left\{ \begin{array}{ll} 2-2c_p\Gamma(2p+1)|\boldsymbol{s}|^{2p} & \text{for } |\boldsymbol{s}| \ll 1\,, \\ 1+\frac{\Gamma(1/(2p+1))}{(2p+1)^{2p/(2p+1)}(2c_p)^{1/(2p+1)}}|\boldsymbol{s}|^{-2p/(2p+1)} & \text{for } |\boldsymbol{s}| \gg 1\,, \end{array} \right.$$

for c_p given by (66). Thus, the profiles both identify the three parameters

$$p\,, \quad \ell_p\,, \quad P_{\rm tot}\,, \tag{84}$$

and we have

$$\ell_p \quad = \quad \left(\frac{\lambda_o L_{\rm att}}{2\pi\ell_x}\right)\left(\frac{\pi^2\sigma^2\ell_z L_{\rm att}}{\lambda_o^2}\right)^{1/2p}\,, \tag{85}$$

$$P_{\rm tot} \quad = \quad \left(\frac{\pi^2\sigma^2\ell_z L_{\rm att}}{\lambda_o^2}\right)\check{\mathcal{C}}_{K_z}(\boldsymbol{0})\Big[\int \left\langle|\check{b}_0(\boldsymbol{x})|^2\right\rangle d\boldsymbol{x}\Big]\,. \tag{86}$$

We remark that if we assume a specific form for the medium correlation function in the longitudinal direction we can identify further medium fluctuation parameters. Assuming for instance the rough ($p=1/2$) Matérn model (57) gives

$$\check{\mathcal{C}}_{K_z}(\boldsymbol{0}) = \frac{\sqrt{2}}{1+8(\pi\ell_z/\lambda_o)^2}\,. \tag{87}$$

Note first that in this rough case the mean reflected power is maximized by choosing the wavelength as small as possible. Note next that if we have measurements at two wavelengths $\{\lambda_o^{(j)}, j=1,2\}$, and identify the corresponding profile parameters in (84), $\{P_{\rm tot}^{(j)}, j=1,2\}$, then we can identify

$$\ell_z^2 \quad = \quad \left(\frac{1}{8\pi^2}\right)\frac{P_{\rm tot}^{(1)}(\lambda_o^{(1)})^2 - P_{\rm tot}^{(2)}(\lambda_o^{(2)})^2}{P_{\rm tot}^{(2)} - P_{\rm tot}^{(1)}}\,. \tag{88}$$

Using the ℓ_z estimate from Eq. (88) to compute $\check{\mathcal{C}}_{K_z}(\boldsymbol{0})$ as in Eq. (87) allows us to identify $\sigma^2\ell_z L_{\rm att}$ from Eq. (86), which subsequently allows us to identify $L_{\rm att}/\ell_x$ from Eq. (85). To summarize, we identify p that characterizes the roughness of the medium fluctuations from the observed profiles in Eqs. (82) and (83). Then using also the other profile parameters at two wavelengths we can identify the medium parameters:

$$\ell_z\,, \quad \sigma^2\ell_x\,, \quad \sigma^2 L_{\rm att}\,.$$

We remark that averaging with respect to the transverse wavevector enhances the signal-to-noise ratio. In addition averaging over several transverse probing positions and frequencies can also be used to enhance the signal-to-noise ratio. In the context of the turbulent atmosphere one can use the time dependence and ergodicity of the medium and repeated probing to enhance the signal-to-noise ratio.

8. **Conclusions.** We have considered the statistics of the wave field reflected by a random medium. We have analyzed how the structure of the enhanced backscattering cone relates to the statistics of the medium. We have analyzed in particular the form of the cone in the case when the medium fluctuations are modeled by the Matérn covariance function. This covariance function is frequently used to model atmospheric turbulence or biological tissue and in the latter context the form of the cone and its dependence on medium fabric have been used to probe for tissue anomaly caused by cancer. An important aspect of the implementation in the case of biological applications is to use low-coherence sources as they serve to enhance the signal-to-noise ratio and we analyze here the situation with sources of this type.

Acknowledgments. This research is supported by AFOSR grant FA9550-18-1-0217 and NSF grant 1616954.

Appendix A. Asymptotic analysis of the reflection operator.

A.1. **Coupled equations.** Using the mode coupling equations (11-12) we find for the reflection and transmission operators introduced in Eqs. (19) and (20)

$$\begin{aligned}\frac{d}{dz}\hat{\mathcal{R}}^\varepsilon(\boldsymbol{k},\boldsymbol{k}',z) &= e^{-2i\frac{\omega}{c_o}\frac{z}{\varepsilon^2}}\hat{\mathcal{L}}^\varepsilon(\boldsymbol{k},\boldsymbol{k}',z) \\ &+e^{2i\frac{\omega}{c_o}\frac{z}{\varepsilon^2}}\iint \hat{\mathcal{R}}^\varepsilon(\boldsymbol{k},\boldsymbol{k}_1,z)\hat{\mathcal{L}}^\varepsilon(\boldsymbol{k}_1,\boldsymbol{k}_2,z)\hat{\mathcal{R}}^\varepsilon(\boldsymbol{k}_2,\boldsymbol{k}',z)d\boldsymbol{k}_1d\boldsymbol{k}_2 \\ &+\int \hat{\mathcal{L}}^\varepsilon(\boldsymbol{k},\boldsymbol{k}_1,z)\hat{\mathcal{R}}^\varepsilon(\boldsymbol{k}_1,\boldsymbol{k}',z)+\hat{\mathcal{R}}^\varepsilon(\boldsymbol{k},\boldsymbol{k}_1,z)\hat{\mathcal{L}}^\varepsilon(\boldsymbol{k}_1,\boldsymbol{k}',z)d\boldsymbol{k}_1\,, \end{aligned} \tag{89}$$

$$\begin{aligned}\frac{d}{dz}\hat{\mathcal{T}}^\varepsilon(\boldsymbol{k},\boldsymbol{k}',z) &= \int \hat{\mathcal{T}}^\varepsilon(\boldsymbol{k},\boldsymbol{k}_1,z)\hat{\mathcal{L}}^\varepsilon(\boldsymbol{k}_1,\boldsymbol{k}',z)d\boldsymbol{k}_1 \\ &+e^{2i\frac{\omega}{c_o}\frac{z}{\varepsilon^2}}\iint \hat{\mathcal{T}}^\varepsilon(\boldsymbol{k},\boldsymbol{k}_1,z)\hat{\mathcal{L}}^\varepsilon(\omega,\boldsymbol{k}_1,\boldsymbol{k}_2,z)\hat{\mathcal{R}}^\varepsilon(\boldsymbol{k}_2,\boldsymbol{k}',z)d\boldsymbol{k}_1d\boldsymbol{k}_2\,, \end{aligned} \tag{90}$$

where we have defined

$$\begin{aligned}\hat{\mathcal{L}}^\varepsilon\big(\boldsymbol{k}_1,\boldsymbol{k}_2,z\big) &= -\frac{ic_o}{2\omega}|\boldsymbol{k}_1|^2\delta(\boldsymbol{k}_1-\boldsymbol{k}_2)+\frac{i\omega}{2(2\pi)^d c_o\varepsilon}\hat{\nu}\Big(\boldsymbol{k}_1-\boldsymbol{k}_2,\frac{z}{\varepsilon^2}\Big) \\ &\quad -\frac{\sigma_o}{2c_o}\delta(\boldsymbol{k}_1-\boldsymbol{k}_2)-\frac{\varepsilon\sigma_o}{2(2\pi)^d c_o}\hat{\mu}\Big(\boldsymbol{k}_1-\boldsymbol{k}_2,\frac{z}{\varepsilon^2}\Big)\,, \end{aligned} \tag{91}$$

with $\hat{\nu}(\boldsymbol{k},z)$ the partial Fourier transform of $\nu(\boldsymbol{x},z)$ (as in (18)). This system is supplemented by the initial conditions

$$\begin{aligned}\hat{\mathcal{R}}^\varepsilon(\boldsymbol{k},\boldsymbol{k}',z=-L) &= 0\,, \\ \hat{\mathcal{T}}^\varepsilon(\boldsymbol{k},\boldsymbol{k}',z=-L) &= \delta(\boldsymbol{k}-\boldsymbol{k}')\,, \end{aligned}$$

corresponding to the boundary conditions (14-15). The reflection operator evaluated at $z=0$ carries all the relevant information about the random medium from the point of view of the reflected wave. We next discuss how we can characterize the second order moments associated with the reflection operator.

A.2. **The second-order moments of the reflection operator.** The reflection operator $\hat{\mathcal{R}}^\varepsilon$ solves (89) with the initial condition (92). It is possible to compute the cross moments of the reflection operator using diffusion approximation theory in the limit $\varepsilon \to 0$, in which the phase factors $\exp(\pm 2i\omega z/(c_o\varepsilon^2))$ act as decoupling terms [11]. We are interested in the second-order moment

$$\mathcal{V}_{(\boldsymbol{k}_1,\boldsymbol{k}_2),(\boldsymbol{k}_3,\boldsymbol{k}_4)}(z) = \lim_{\varepsilon\to 0} \mathbb{E}\left[\hat{\mathcal{R}}^\varepsilon(\boldsymbol{k}_1,\boldsymbol{k}_2,z)\overline{\hat{\mathcal{R}}^\varepsilon}(\boldsymbol{k}_3,\boldsymbol{k}_4,z)\right], \tag{92}$$

at the surface $z = 0$ in the regime of weak backscattering. This regime derives from the hypothesis in Eq. (21) where $\widehat{C}(\boldsymbol{k},K) = \sigma^2\ell_z\ell_x^d\widehat{\mathcal{C}}_{K\ell_z}(\boldsymbol{k}\ell_x)$. We have up to terms of order δ^2 the following result (this is a straightforward generalization of Proposition 2 in [11] for the case without attenuation).

Proposition 5. *In the weak backscattering regime (21) the limit moments $\mathcal{V}_{(\boldsymbol{k}_1,\boldsymbol{k}_2),(\boldsymbol{k}_3,\boldsymbol{k}_4)}$ are given by the system of equations*

$$\begin{aligned}
\frac{\partial \mathcal{V}_{(\boldsymbol{k}_1,\boldsymbol{k}_2),(\boldsymbol{k}_3,\boldsymbol{k}_4)}}{\partial z} &= -\frac{2\sigma_o}{c_o}\mathcal{V}_{(\boldsymbol{k}_1,\boldsymbol{k}_2),(\boldsymbol{k}_3,\boldsymbol{k}_4)} \\
&+\frac{ic_o}{2\omega}\Big[-\big(|\boldsymbol{k}_1|^2+|\boldsymbol{k}_2|^2\big)+\big(|\boldsymbol{k}_3|^2+|\boldsymbol{k}_4|^2\big)\Big]\mathcal{V}_{(\boldsymbol{k}_1,\boldsymbol{k}_2),(\boldsymbol{k}_3,\boldsymbol{k}_4)} \\
&+\frac{\omega^2}{4(2\pi)^d c_o^2}\int \widehat{C}(\boldsymbol{k},0)\Big\{\mathcal{V}_{(\boldsymbol{k}_1-\boldsymbol{k},\boldsymbol{k}_2),(\boldsymbol{k}_3-\boldsymbol{k},\boldsymbol{k}_4)}+\mathcal{V}_{(\boldsymbol{k}_1,\boldsymbol{k}_2-\boldsymbol{k}),(\boldsymbol{k}_3,\boldsymbol{k}_4-\boldsymbol{k})} \\
&\qquad +\mathcal{V}_{(\boldsymbol{k}_1-\boldsymbol{k},\boldsymbol{k}_2),(\boldsymbol{k}_3,\boldsymbol{k}_4+\boldsymbol{k})}+\mathcal{V}_{(\boldsymbol{k}_1,\boldsymbol{k}_2-\boldsymbol{k}),(\boldsymbol{k}_3+\boldsymbol{k},\boldsymbol{k}_4)} \\
&\qquad -\mathcal{V}_{(\boldsymbol{k}_1-\boldsymbol{k},\boldsymbol{k}_2-\boldsymbol{k}),(\boldsymbol{k}_3,\boldsymbol{k}_4)}-\mathcal{V}_{(\boldsymbol{k}_1,\boldsymbol{k}_2),(\boldsymbol{k}_3-\boldsymbol{k},\boldsymbol{k}_4-\boldsymbol{k})} \\
&\qquad -2\mathcal{V}_{(\boldsymbol{k}_1,\boldsymbol{k}_2),(\boldsymbol{k}_3,\boldsymbol{k}_4)}\Big\}\,d\boldsymbol{k} \\
&+\frac{\omega^2}{4(2\pi)^d c_o^2}\widehat{C}\Big(\boldsymbol{k}_1-\boldsymbol{k}_2,\frac{2\omega}{c_o}\Big)\,\delta(\boldsymbol{k}_1-\boldsymbol{k}_2-\boldsymbol{k}_3+\boldsymbol{k}_4)\,,
\end{aligned} \tag{93}$$

starting from $\mathcal{V}_{(\boldsymbol{k}_1,\boldsymbol{k}_2),(\boldsymbol{k}_3,\boldsymbol{k}_4)}(z=-L)=0$.

We can observe that $\mathcal{V}_{(\boldsymbol{k}_1,\boldsymbol{k}_2),(\boldsymbol{k}_3,\boldsymbol{k}_4)}$ is supported on $\boldsymbol{k}_1-\boldsymbol{k}_2-\boldsymbol{k}_3+\boldsymbol{k}_4=\boldsymbol{0}$ so that we can parameterize the solution in terms of three wavevectors. We then obtain Proposition 1.

Appendix B. Asymptotic expressions for the cross spectral density.

In the next two lemmas we give the asymptotic expressions for the dimensionless cross spectral density $\mathcal{D}$ in the regime $\alpha \gg 1$.

Lemma B.1. *1. There exists C_β such that $\sup_{\boldsymbol{u},\boldsymbol{v},\boldsymbol{w}\in\mathbb{R}^d}|\mathcal{D}(\boldsymbol{u},\boldsymbol{v},\boldsymbol{w},0)| \le C_\beta$ uniformly in α.*

2. If $\boldsymbol{u}\cdot\boldsymbol{v}\neq 0$, then $\lim_{\alpha\to\infty}\mathcal{D}(\boldsymbol{u},\boldsymbol{v},\boldsymbol{w},0)=0$.

3. If $\boldsymbol{u}\neq\boldsymbol{0}$, $\boldsymbol{v}\neq\boldsymbol{0}$, and $\boldsymbol{u}\cdot\boldsymbol{v}=0$, then

$$\lim_{\alpha\to\infty}\mathcal{D}(\boldsymbol{u},\boldsymbol{v},\boldsymbol{w},0)=\frac{\widehat{\mathcal{C}}_{K_z}(\boldsymbol{w})}{\check{\mathcal{C}}_{K_z}(\boldsymbol{0})}\frac{1-e^{-[1+2\beta\check{\mathcal{C}}_0(\boldsymbol{0})]\zeta_L}}{1+2\beta\check{\mathcal{C}}_0(\boldsymbol{0})}\,. \tag{94}$$

4. If $\boldsymbol{u}=\boldsymbol{0}$ and $\boldsymbol{v}\neq\boldsymbol{0}$, then $\lim_{\alpha\to\infty}\mathcal{D}(\boldsymbol{0},\boldsymbol{v},\boldsymbol{w},0)=\mathcal{D}_{\boldsymbol{0}}(\boldsymbol{w},0)$, where $\mathcal{D}_{\boldsymbol{0}}(\boldsymbol{w},\zeta)$ is the solution of

$$\begin{aligned}
\frac{d\mathcal{D}_{\boldsymbol{0}}(\boldsymbol{w},\zeta)}{d\zeta} &= \frac{\widehat{\mathcal{C}}_{K_z}(\boldsymbol{w})}{\check{\mathcal{C}}_{K_z}(\boldsymbol{0})}-\mathcal{D}_{\boldsymbol{0}}(\boldsymbol{w},\zeta) \\
&+\frac{2\beta}{(2\pi)^d}\int\widehat{\mathcal{C}}_0(\boldsymbol{\mu})\left[\mathcal{D}_{\boldsymbol{0}}(\boldsymbol{w}+\boldsymbol{\mu},\zeta)-\mathcal{D}_{\boldsymbol{0}}(\boldsymbol{w},\zeta)\right]d\boldsymbol{\mu}\,,
\end{aligned} \tag{95}$$

starting from $\mathcal{D}_{\mathbf{0}}(\boldsymbol{w},\zeta=-\zeta_L)=0$.

5. *If* $\boldsymbol{u}\neq\mathbf{0}$ *and* $\boldsymbol{v}=\mathbf{0}$, *then* $\lim_{\alpha\to\infty}\mathcal{D}(\boldsymbol{u},\mathbf{0},\boldsymbol{w},0)=\mathcal{D}_{\mathbf{0}}(\boldsymbol{w},0)$.
6. *If* $\boldsymbol{u}=\mathbf{0}$ *and* $\boldsymbol{v}=\mathbf{0}$, *then* $\lim_{\alpha\to\infty}\mathcal{D}(\mathbf{0},\mathbf{0},\boldsymbol{w},0)=\mathcal{D}_{\mathbf{0},\mathbf{0}}(\boldsymbol{w},0)$ *with*

$$\mathcal{D}_{\mathbf{0},\mathbf{0}}(\boldsymbol{w},0)=2\mathcal{D}_{\mathbf{0}}(\boldsymbol{w},0)-\frac{\widehat{\mathcal{C}}_{K_z}(\boldsymbol{w})}{\check{\mathcal{C}}_{K_z}(\mathbf{0})}\frac{1-e^{-[1+2\beta\check{\mathcal{C}}_0(\mathbf{0})]\zeta_L}}{1+2\beta\check{\mathcal{C}}_0(\mathbf{0})}\,. \tag{96}$$

By comparing the third and fourth items (or the fifth and sixth items) a sharp transition is noticed from the case $\boldsymbol{u}=\mathbf{0}$ to $\boldsymbol{u}\neq\mathbf{0}$. This transition can be studied in detail by looking at small $\boldsymbol{u}$ of order α^{-1}, and we then find

Lemma B.2. 1. *If* $\boldsymbol{v}\neq\mathbf{0}$, *then* $\lim_{\alpha\to\infty}\mathcal{D}(\alpha^{-1}\boldsymbol{s},\boldsymbol{v},\boldsymbol{w},0)=\mathcal{D}_{\boldsymbol{s}}(\boldsymbol{v},\boldsymbol{w},0)$ *where* $\mathcal{D}_{\boldsymbol{s}}(\boldsymbol{v},\boldsymbol{w},\zeta)$ *is solution of*

$$\begin{aligned}\frac{d\mathcal{D}_{\boldsymbol{s}}(\boldsymbol{v},\boldsymbol{w},\zeta)}{d\zeta} &= \frac{\widehat{\mathcal{C}}_{K_z}(\boldsymbol{w})}{\check{\mathcal{C}}_{K_z}(\mathbf{0})}e^{i\boldsymbol{s}\cdot\boldsymbol{v}\zeta}-\big[1+2\beta\check{\mathcal{C}}_0(\mathbf{0})\big]\mathcal{D}_{\boldsymbol{s}}(\boldsymbol{v},\boldsymbol{w},\zeta)\\ &\quad+\frac{\beta}{(2\pi)^d}\int\widehat{\mathcal{C}}_0(\boldsymbol{\mu})\big[e^{i\boldsymbol{s}\cdot\boldsymbol{\mu}\zeta}\mathcal{D}_{\boldsymbol{s}}(\boldsymbol{v}-\boldsymbol{\mu},\boldsymbol{w}+\boldsymbol{\mu},\zeta)\\ &\quad+e^{-i\boldsymbol{s}\cdot\boldsymbol{\mu}\zeta}\mathcal{D}_{\boldsymbol{s}}(\boldsymbol{v}+\boldsymbol{\mu},\boldsymbol{w}+\boldsymbol{\mu},\zeta)\big]d\boldsymbol{\mu}\,,\end{aligned} \tag{97}$$

starting from $\mathcal{D}_{\boldsymbol{s}}(\boldsymbol{v},\boldsymbol{w},\zeta=-\zeta_L)=0$.

2. *If* $\boldsymbol{v}=\mathbf{0}$, *then* $\lim_{\alpha\to\infty}\mathcal{D}(\alpha^{-1}\boldsymbol{s},\mathbf{0},\boldsymbol{w},0)=\mathcal{D}_{\boldsymbol{s},\mathbf{0}}(\boldsymbol{w},0)$ *with*

$$\mathcal{D}_{\boldsymbol{s},\mathbf{0}}(\boldsymbol{w},0)=\mathcal{D}_{\boldsymbol{s}}(\mathbf{0},\boldsymbol{w},0)+\mathcal{D}_{\mathbf{0}}(\boldsymbol{w},0)-\frac{\widehat{\mathcal{C}}_{K_z}(\boldsymbol{w})}{\check{\mathcal{C}}_{K_z}(\mathbf{0})}\frac{1-e^{-[1+2\beta\check{\mathcal{C}}_0(\mathbf{0}])\zeta_L}}{1+2\beta\check{\mathcal{C}}_0(\mathbf{0})}\,. \tag{98}$$

Note that $\mathcal{D}_{\boldsymbol{s}}(\boldsymbol{v},\boldsymbol{w},0)\,|_{\boldsymbol{s}=\mathbf{0}}=\mathcal{D}_{\mathbf{0}}(\boldsymbol{w},0)$ as defined by (95). By solving the differential equation (97) we obtain the following integral representation of $\mathcal{D}_{\boldsymbol{s}}(\boldsymbol{v},\boldsymbol{w},\zeta)$ valid for all $\boldsymbol{s}\in\mathbb{R}^d$:

$$\begin{aligned}\mathcal{D}_{\boldsymbol{s}}(\boldsymbol{v},\boldsymbol{w},\zeta) &= \int\frac{\check{\mathcal{C}}_{K_z}(\boldsymbol{\lambda})}{\check{\mathcal{C}}_{K_z}(\mathbf{0})}e^{-i\boldsymbol{w}\cdot\boldsymbol{\lambda}}\int_{-\zeta_L}^{\zeta}e^{i\boldsymbol{v}\cdot\boldsymbol{s}\zeta'}\\ &\quad\times e^{\beta\int_{\zeta'}^{\zeta}\check{\mathcal{C}}_0(\boldsymbol{\lambda}-\boldsymbol{s}\zeta'')+\check{\mathcal{C}}_0(\boldsymbol{\lambda}+\boldsymbol{s}\zeta'')-2\check{\mathcal{C}}_0(\mathbf{0})d\zeta''-(\zeta-\zeta')}\,d\zeta' d\boldsymbol{\lambda}\,.\end{aligned} \tag{99}$$

When $\boldsymbol{s}=\mathbf{0}$ the function $\mathcal{D}_{\boldsymbol{s}}(\boldsymbol{v},\boldsymbol{w},\zeta)$ is independent of $\boldsymbol{v}$ and we have

$$\mathcal{D}_{\mathbf{0}}(\boldsymbol{w},\zeta)=\int\frac{\check{\mathcal{C}}_{K_z}(\boldsymbol{\lambda})}{\check{\mathcal{C}}_{K_z}(\mathbf{0})}e^{-i\boldsymbol{w}\cdot\boldsymbol{\lambda}}\int_0^{\zeta_L+\zeta}e^{-\zeta'+2\beta[\check{\mathcal{C}}_0(\boldsymbol{\lambda})-\check{\mathcal{C}}_0(\mathbf{0})]\zeta'}\,d\zeta' d\boldsymbol{\lambda}\,. \tag{100}$$

As a result we get the following lemma.

Lemma B.3. *When* $L\gg L_{\rm att}$ *we have*

$$\begin{aligned}\mathcal{D}_{\boldsymbol{s}}(\boldsymbol{v},\boldsymbol{w},0) &= \int\frac{\check{\mathcal{C}}_{K_z}(\boldsymbol{\lambda})}{\check{\mathcal{C}}_{K_z}(\mathbf{0})}e^{-i\boldsymbol{w}\cdot\boldsymbol{\lambda}}\int_0^{\infty}e^{-i\boldsymbol{v}\cdot\boldsymbol{s}\zeta}\\ &\quad\times e^{\beta\int_0^{\zeta}\check{\mathcal{C}}_0(\boldsymbol{\lambda}-\boldsymbol{s}\zeta')+\check{\mathcal{C}}_0(\boldsymbol{\lambda}+\boldsymbol{s}\zeta')-2\check{\mathcal{C}}_0(\mathbf{0})d\zeta'-\zeta}\,d\zeta d\boldsymbol{\lambda}\,,\end{aligned} \tag{101}$$

and

$$\mathcal{D}_{\mathbf{0}}(\boldsymbol{w},0)=\int\frac{\check{\mathcal{C}}_{K_z}(\boldsymbol{\lambda})}{\check{\mathcal{C}}_{K_z}(\mathbf{0})}e^{-i\boldsymbol{w}\cdot\boldsymbol{\lambda}}\frac{1}{1+2\beta[\check{\mathcal{C}}_0(\mathbf{0})-\check{\mathcal{C}}_0(\boldsymbol{\lambda})]}d\boldsymbol{\lambda}\,. \tag{102}$$

We use these expressions in the paper to study the reflected intensity profiles and the enhanced backscattering cone, specifically to derive Propositions 3 and 4.

Appendix C. Notations.

c_o	background speed of propagation of the medium
σ_o	background attenuation of the medium
ℓ_z	longitudinal correlation radius of the random medium
ℓ_x	transverse correlation radius of the random medium
σ	standard deviation of the random medium
ω	(angular) frequency of the source
r_0	radius of the source
ρ_0	correlation radius of the source
$\boldsymbol{k}_0$	transverse wavevector of the source
$\lambda_o = \dfrac{2\pi c_o}{\omega}$	wavelength
$L_{\rm att} = \dfrac{c_o}{2\sigma_o}$	attenuation length
$\zeta_L = \dfrac{L}{L_{\rm att}}$	relative propagation distance
$K_z = \dfrac{2\omega\ell_z}{c_o}$	relative wavenumber
$\alpha = \dfrac{c_o^2}{2\sigma_o\omega\ell_x^2}$	strength of diffraction
$\beta = \dfrac{\omega^2\sigma^2\ell_z}{8c_o\sigma_o}$	strength of forward scattering
$\overline{D}_o$	cross spectral density central value (see Eq. (26))
$P_{\rm tot}$	mean reflected power (see Eq. (31))

TABLE 1. Notations used in the paper.

REFERENCES

[1] V. A. Banakh and I. N. Smalikho, Determination of optical turbulence intensity by atmospheric backscattering of laser radiation, *Atmospheric and Oceanic Optics*, **24** (2011), 457.

[2] Y. N. Barabanenkov, Wave corrections for the transfer equation for backward scattering, *Izv. Vyssh. Uchebn. Zaved. Radiofiz.,* **16** (1973), 88–96.

[3] R. Bi, J. Dong and K. Lee, Coherent backscattering cone shape depends on the beam size, *Appl. Optics*, **51** (2012), 6301–6306.

[4] I. R. Capoglu, J. D. Rogers, A. Taflove and V. Backman, Accuracy of the Born approximation in calculating the scattering coefficient of biological continuous random media, *Opt. Lett.*, **34** (2009), 2679–2681.

[5] J. Chrzanowski, J. Kirkiewicz and Yu. A. Kravtsov, Influence of enhanced backscattering phenomenon on laser measurements of dust and aerosols content in a turbulent atmosphere, *Phys. Lett. A*, **300** (2002), 298–302.

[6] J. H. Churnside and J. J. Wilson, Enhanced backscatter of a reflected beam in atmospheric turbulence, *Appl Opt.*, **32** (1993), 2651–2655.

[7] M. V. de Hoop, J. Garnier and K. Sølna, Enhanced and specular backscattering in random media, *Waves in Random and Complex Media*, **22** (2012), 505–530.

[8] D. de Wolf, Electromagnetic reflection from an extended turbulent medium: Cumulative forward-scatter single-backscatter approximation, *IEEE Trans. Antennas Propagat*, **19** (1971), 254–262.

[9] D. de Wolf, Discussion of radiatlve transfer methods applied to electromagnetic reflection from turbulent plasma, *IEEE Trans. Antennas Propagat*, **20** (1972), 805–807.

[10] J.-P. Fouque, J. Garnier, G. Papanicolaou and K. Sølna, *Wave Propagation and Time Reversal in Randomly Layered Media,* Springer, New York, 2007.

[11] J. Garnier and K. Sølna, Random backscattering in the parabolic scaling, *J. Stat. Phys.*, **131** (2008), 445–486.

[12] J. Garnier and K. Sølna, Coupled paraxial wave equations in random media in the white-noise regime, *Ann. Appl. Probab.*, **19** (2009), 318–346.

[13] J. Garnier and K. Sølna, Wave backscattering by point scatterers in the random paraxial regime, *SIAM J. Multiscale Model. Simul.*, **3** (2014), 1309–1334.
[14] J. Garnier and K. Sølna, White-noise paraxial approximation for a general random hyperbolic system, *SIAM J. Multiscale Model. Simul.*, **13** (2015), 1022–1060.
[15] J. Garnier and K. Sølna, Fourth-moment Analysis for wave propagation in the white-noise paraxial regime, *Arch. Rat. Mech. Anal.*, **220** (2016), 37–81.
[16] J. Garnier and K. Sølna, Imaging through a scattering medium by speckle intensity correlations over incident angle, *Inverse Problems*, **34** (2018), 094003, 22pp.
[17] J. Garnier and K. Sølna, Non-invasive imaging through random media, *SIAM J. Appl. Math.*, **78** (2018), 3296–3315.
[18] A. K. Glaser, Y. Chen and J. T. C. Liu, Fractal propagation method enables realistic optical microscopy simulations in biological tissues, *Optica*, **3** (2016), 861–869.
[19] K. S. W. Gong and C. J. R. Shappard, Model for light scattering in biological tissue and cells based on random rough nonspherical particles, *Appl. Optics*, **48** (2009), 1153–1157.
[20] Y. L. Kim, Y. Liu, V. M. Turzhitsky, H. K. Roy, R. K. Wali and V. Backman, Coherent backscattering spectroscopy, *Opt. Lett.*, **29** (2004), 1906–1908.
[21] Y. L. Kim, Y. Liu, V. M. Turzhitsky, H. K. Roy, R. K. Wali, P. P. Subramanian, P. Pradhan and V. Backman, Low-coherence enhanced backscattering: Review of principles and applications for colon cancer screening, *J. Biomed. Opt.*, **11** (2006), 041125.
[22] Y. L. Kim, Y. Liu, V. M. Turzhitsky, R. K. Wali, H. K. Roy and V. Backman, Depth-resolved low-coherence enhanced backscattering, *Opt. Lett.*, **30** (2007), 741–743.
[23] G. Labeyrie, F. de Tomasi, J.-C. Bernard, C. A. Müller, C. Miniatura and R. Kaiser, Coherent backscattering of light by atoms, *Phys. Rev. Lett.*, **83** (1999), 5266–5269.
[24] J. Liu, Z. Xu, Q. Song, R. L. Konger and Y. L. Kim, Enhancement factor in low-coherence enhanced backscattering and its applications for characterizing experimental skin carcinogenesis, *J. Biomed. Opt.*, **15** (2010), 037011.
[25] N. Mutyal, A. Radosevich, B. Gould, J. D. Rodgers, A. Gomes, V. Turzhitsky and V. Backman, A fiber optic probe design to measure depth- limited optical properties in-vivo with with Low-coherence Enhanced Backscattering (LEBS) Spectroscopy, *Opt. Express*, **20** (2012), 19643–19657.
[26] J. P. Nolan, Multivariate elliptically contoured stable distributions: Theory and estimation, *Computational Statistics*, **28** (2013), 2067–2089.
[27] A. J. Radosevisch, N. M. Nikhil, J. D. Rogers, B. Gould, T. A. Hensing, D. Ray, V. Backman and H. K. Roy, Buccal spectral markers for lung cancer risk stratification, *Plos One*, **9** (2014), e10157.
[28] J. D. Rogers, I. R. Capoglu and V. Backman, Nonscalar elastic light scattering from continuous random media in the Born approximation, *Opt. Lett.*, **34** (2009), 1891–1893.
[29] J. D. Rogers, A. J. Radosevich, J. Yi and V. Backman, Modeling light scattering in tissue as continuous random media using a versatile refractive index correlation function, *IEEE J. Sel. Top. Quant.*, **20** (2014), 7000514.
[30] Y. M. Sebrebrennikova and L. H. Garcia-Rubio, Modeling and interpretation of extinction spectra of oriented nonspherical composite particles: application to biological cells, *Appl. Optics*, **49** (2010), 4460–4471.
[31] C. J. R. Sheppard, Fractal model of light scattering in biological tissue and cells, *Opt. Lett.*, **32** (2007), 142–144.
[32] A. Tourin, A. Derode, P. Roux, B. A. van Tiggelen and M. Fink, Time-dependent coherent backscattering of acoustic waves, *Phys. Rev. Lett.,* **79** (1997), 3637–3639.
[33] V. Turzhitsky, A. J. Radosevich, J. D. Rogers, N. N. Mutyal and V. Backman, Measurement of optical scattering properties with low-coherence enhanced backscattering spectroscopy, *J. Biomed. Opt.*, **16** (2011), 067007.
[34] V. Turzhitsky, J. D. Rogers, N. N. Mutyal, H. K. Roy and V. Backman, Characterization of light transport in scattering media at subdiffusion length scales with Low-coherence Enhanced Backscattering, *IEEE J. Sel. Top. Quant.*, **16** (2010), 619–626.
[35] M. P. van Albada and A. Lagendijk, Observation of weak localization of light in a random medium, *Phys. Rev. Lett.*, **55** (1985), 2692–2695.
[36] M. C. W. van Rossum and Th. M. Nieuwenhuizen, Multiple scattering of classical waves: Microscopy, mesoscopy, and diffusion, *Rev. Mod. Phys.*, **71** (1999), 313–371.
[37] P. E. Wolf and G. Maret, Weak localization and coherent backscattering of photons in disordered media, *Phys. Rev. Lett.*, **55** (1985), 2696–2699.

[38] P. E. Wolf, G. Maret, E. Akkermans and R. Maynard, Optical coherent backscattering by random media: An experimental study, *Journal de Physique*, **49** (1988), 63–75.
[39] M. Xu and R. R. Alfano, Fractal mechanisms of light scattering in biological tissue and cells, *Opt. Lett.*, **30** (2005), 3051–3053.
[40] K. M. Yoo, G. C. Tang and R. R. Alfano, Coherent backscattering of light from biological tissues, *Appl. Opt.*, **29** (1990), 3237–3239.

Received September 2019; revised February 2020.

E-mail address: josselin.garnier@polytechnique.edu
E-mail address: ksolna@math.uci.edu